Pergamon

Chemical Engineering Science, Vol. 53, No. 19, pp. 3413–3434, 1998

Printed in Great Britain

PII: S0009–2509(98)00137–7

0009–2509/98/$–See front matter

Stokes flow caused by the motion of a rigid sphere close to a viscous interface

K. D. Danov,* T. D. Gurkov,* H. Raszillier† and F. Durst†‡

*Laboratory of Thermodynamics and Physico-Chemical Hydrodynamics, Faculty of Chemistry, University of Sofia, James Bourchier Avenue 1, Sofia 1126, Bulgaria;

†Lehrstuhl für Strömungsmechanik, Technische Fakultät, Universität Erlangen-Nürnberg, Cauerstraße 4, D-91058 Erlangen, Germany

(Received 9 April 1997; accepted 20 May 1998)

Abstract—The subject of this work is the creeping motion of liquid caused by steady translation and rotation of a solid sphere close to an interface between two fluid phases. The case of vanishingly small Reynolds and capillary numbers is considered. We account for the intrinsic viscous properties of the liquid boundary, characterised by dilatational and shear *surface* viscosities, in the frame of the Boussinesq–Scriven model. Numerical computations are presented for the velocity and pressure distributions throughout the flow domain. The drag force and the torque exerted on the particle are obtained by means of analytical integration of the stresses over the spherical surface. At small distances of separation between the rigid sphere and the wall, the role of the surface viscosity becomes quite substantial: the drag and the toque can be several times bigger than those which correspond to motion in an unbounded fluid. For steady rotation the flow around the solid particle is restrained in a relatively narrow region, whereas with translation the velocity field extends to large distances. Consequently, the rotating sphere should be closer in order to start 'feeling' the wall. Our results are relevant for systems which contain surfactant laden interfaces. We showed that even with low molecular weight surfactants such interfaces can behave much like *solid* ones. This is particularly true for fluid boundaries covered by proteins, as they turn out to be completely immobilised.

Keywords: Interface; surface viscosity; creeping flow; drag and torque on sphere.

1. INTRODUCTION

The flow of viscous liquid, resulting from the motion of an immersed particle, can be substantially affected by the presence of walls. This situation has important implications in a variety of engineering problems, such as suspension flows in pipes, or coating processes. Earlier works devoted to theoretical investigation of the impact of plane and cylindrical walls on the creeping motion of liquid around a particle (at low Reynolds numbers and negligible inertia) were reviewed by Happel and Brenner (1965). One possible approach to this task is to represent the forces and torques exerted on the particle as power series in terms of the ratio between the characteristic particle size, a, and its distance to the wall, l. In other words, one can seek for consecutive corrections to the case of flow in an unbounded liquid. When the quotient a/l is small, the so-called method of reflections is applicable (Kim and Karrila, 1991). An iteration procedure consists of applying the boundary conditions separately, and in succession, on one surface at a time. The latter method was used for the first time by Smoluchowski (1911), and was further developed by Faxén (1921) and Wakiya (1956), who studied the motion of a sphere in a liquid layer confined between two flat solid walls.

Another approach was proposed by Dean and O'Neill (1963) and O'Neill (1964). They considered a spherical rigid particle undergoing parallel translational and rotational motion in the vicinity of a plane hard wall. Specific bipolar coordinates were used, which allowed the authors to impose boundary conditions on both surfaces simultaneously. Thus, exact solutions, expressed in terms of infinite series of Legendre functions, were derived for the velocity and pressure distributions. As pointed out by Goldman *et al.* (1967), these solutions converge poorly (in a numerical sense) if the ratio of gap width to sphere radius is very small (for instance, below 0.001). Some errors made by Dean and O'Neill (1963) in computation were corrected by Goldman *et al.* (1967). The latter work utilised the method of matched asymptotic expansions to explore the limit when the gap width tends to zero. Such kind of treatment was performed

‡Corresponding author.

also by O'Neill and Stewartson (1967), and by Cooley and O'Neill (1968). Lee and Leal (1980) extended the theory of Dean and O'Neill (1963) and O'Neill (1964) by investigating the case when the solid sphere is situated close to a flat surface between two immiscible viscous liquids. Further, Berdan and Leal (1982) showed that such an interface is subject to small deformations, which in turn influence the drag experienced by the particle (the torque is not affected, to a first-order approximation).

Shapira and Haber (1988, 1990) studied the impact of the containing walls on the low Reynolds number hydrodynamics of a droplet moving between two parallel plates in a quiescent fluid, as well as in shear flow. O'Neill and Ranger (1979) derived an exact solution for the velocity field induced by a sphere rotating near an interface that separates two viscous fluids.

All those works considered either solid surfaces, or liquid boundaries which *do not* possess their own intrinsic viscous properties. On the other hand, it was long ago that Boussinesq (1913) introduced the concept of surface viscosity and Scriven (1960) formulated the general constitutive relation for the viscous stresses on Newtonian interfaces of arbitrary shape. This was done by analogy with the three-dimensional case of bulk fluids, postulating the existence of independent dilatational and shear *interfacial* viscosities. These two quantities, although usually negligible on bare surfaces between fluids, turned out to be of major importance when surfactants are adsorbed on the phase boundary (Edwards *et al.*, 1991). Particularly large stresses due to viscous friction within the surface can be anticipated if the latter is covered by proteins. As shown by Graham and Phillips (1980a, b), protein layers exhibit dilatational and shear viscosities which are orders of magnitude larger than those corresponding to low molecular weight surfactants.

Recently Danov *et al.* (1995) studied the slow motion of a solid particle confined in a thin liquid layer whose interfaces are viscous. Direct numerical solution was implemented for the Stokes equations written in the original 'two vorticities–one velocity' formulation. The surface viscosity was found to affect the flow properties considerably.

The purpose of the present article is to investigate the case when a solid sphere moves parallel to a single flat *viscous* interface between two immiscible fluids. We apply the method which was originally proposed by Dean and O'Neill (1963), O'Neill (1964), and was subsequently elaborated by Lee and Leal (1980). The treatment is restricted to slow motions, that is, small Reynolds and capillary numbers. In bipolar coordinates of revolution, the analytical solutions for the fields of velocity and pressure are expressed in terms of infinite series of associated Legendre functions. The boundary conditions furnish some relations between the coefficients in the series. Those coefficients are then obtained by solving a set of linear equations numerically. On the liquid interface the boundary conditions include stress balances which account for the existence of dilatational and shear surface viscosity. Explicit results for the drag and torque are derived by means of analytical integration of forces and moments over the particle surface. Calculations are presented for different values of the interfacial viscosity parameters.

2. STATEMENT OF THE PROBLEM AND GENERAL SOLUTION

We consider a rigid sphere moving in a quiescent fluid (region Ω_1) close to the planar interface (S_2) beyond which there is another bulk fluid phase (Ω_2)—Fig. 1. The particle radius is a, and its surface is denoted by S_1. The sphere can either translate with constant velocity V, parallel to the plane and along the Oy-axis, or rotate with fixed angular velocity ω, the axis of rotation being Ox. The particle–wall distance, d, is fixed. The two bulk fluids are assumed to be homogeneous, isothermal, Newtonian and incompressible. In the volume phase Ω_k the pressure is p_k, the velocity is $\mathbf{v}_k$, and the dynamic viscosity is η_k ($k = 1, 2$). The case of low Reynolds number will be studied, so that the inertia terms in the momentum equations are neglected. In many practically encountered systems, such as coating flows and suspensions, the characteristic particle size is about 1 μm or less, and the relative velocity is of the order of a few cm/s, or less. Therefore, with common liquids (and water) the Reynolds number will be indeed small. In these conditions the flow is governed by the Stokes' equations for creeping motion

$$\nabla p_k = \eta_k \nabla^2 \mathbf{v}_k \tag{1}$$

$$\nabla \cdot \mathbf{v}_k = 0 \quad (k = 1, 2) \tag{2}$$

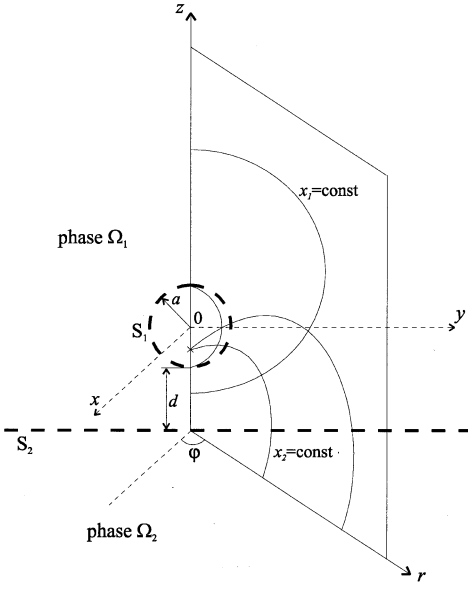

Fig. 1. Schematic picture of the studied system configuration. The curves drawn in the meridional plane (φ = const) represent coordinate lines in the chosen bipolar coordinates, x_1, x_2.

where ∇ is the three-dimensional gradient operator. The general form of the solution of eqs (1) and (2) in the particular geometry (Fig. 1) was given by Dean and O'Neill (1963), O'Neill (1964), Lee and Leal (1980), together with the boundary conditions on flat interface which is solid or liquid with *no intrinsic viscous* properties. For better understanding of our results we believe it is necessary to recapitulate briefly the main equations obtained when working out the problem. This is done below.

Let us denote by $Oxyz$ the system of Cartesian coordinates whose origin coincides with the centre of the particle (Fig. 1). Cylindrical coordinates, r, φ, z, can be introduced, with φ being the meridional angle. Any plane for which φ is constant will be called meridional plane; r and z are, respectively, the radial and the vertical coordinates. The particle motion is assumed to be sufficiently slow, so that the shape perturbation of the liquid–liquid phase boundary (S_2), caused by the pressures on both sides, will be very small. As shown below, such is the case when the capillary number is much less than unity. Then the boundary conditions can be linearised, with the zeroth-order approximation referring to perfectly flat interface. For that reason, we shall consider the problem with non-perturbed surface and shall finally calculate the first-order correction to the shape of S_2.

The solutions of eqs (1), (2) for the velocity and pressure can be expressed as follows (Dean and O'Neill, 1963; O'Neill, 1964):

$$v_{r,k} = V_* R_k(r, z)\sin\varphi, \quad v_{\varphi,k} = V_* F_k(r, z)\cos\varphi,$$
$$v_{z,k} = V_* Z_k(r, z)\sin\varphi \tag{3}$$

$$p_k = \frac{\eta_k V_*}{a} P_k(r, z)\sin\varphi, \quad k = 1, 2 \tag{4}$$

where $v_{r,k}$, $v_{\varphi,k}$ and $v_{z,k}$ are the three velocity components, corresponding to the bulk phase k, in the cylindrical coordinate system $Or\varphi z$. The dimensionless functions R_k, F_k, Z_k and P_k depend on r and z only. V_* is a characteristic velocity, which is equal to V in the case of translation, and $V_* = \omega a$ for rotation. Here and hereafter the radial and vertical coordinates, r, z, are made dimensionless by scaling with the sphere radius, a. Equations (3), (4) may be regarded as a trial solution, suggested by the boundary conditions (cf. Goldman *et al.*, 1967). The specific dependence upon φ allows to reduce the dimensionality of the problem from 3 to 2, as the meridional angle φ is excluded from eqs (1) and (2).

In cylindrical coordinates the particle surface and the unperturbed flat interface are described by the following equations:

$$S_1\colon\ r^2 + z^2 = 1, \quad S_2\colon\ z = -(1 + d) \tag{5}$$

with d being the dimensionless gap width (distance between the closest points of the sphere and the plane, Fig. 1). It is convenient to introduce bipolar coordinates of revolution, as proposed by Dean and O'Neill (1963) and O'Neill (1964). In the meridional plane $\varphi = \text{const}$ we exchange r and z with x_1, x_2:

$$r = \frac{\sin x_2}{h}, \quad z = -(1 + d) - \frac{\sinh x_1}{h}. \tag{6}$$

The metric coefficient h is

$$h = \frac{1}{b}(\cosh x_1 - \cos x_2), \quad b = \sqrt{d(2 + d)}. \tag{7}$$

The coordinate lines $x_1 = \text{const}$ and $x_2 = \text{const}$ are mutually orthogonal circular circumferences whose centers lie on the axes Oz and Or, respectively. In addition, possible values of x_2 are $0 \leqslant x_2 \leqslant \pi$, where $x_2 = \pi$ corresponds to that part of the Oz-axis which is contained between the two poles, $z = -(1 + d) \pm b$. The rest of the line Oz refers to $x_2 = 0$. The curves $x_1 = \text{const}$ and $x_2 = \text{const}$ in the meridional plane generate coordinate surfaces of revolution by means of rotation around Oz. In this coordinate system the equations of the two boundary surfaces, S_1 and S_2, acquire the following form:

$$S_1\colon\ x_1 = -c, \quad S_2\colon\ x_1 = 0, \quad c = \ln(1 + d + b) \tag{8}$$

which can be obtained from eqs (5)–(7). The bulk region Ω_1 is described by $-c < x_1 < 0$, whereas in the volume Ω_2 one has $0 < x_1$.

Solution of the Stokes' problem (1)–(4) is found after introducing auxiliary functions of r and z (cf. Dean and O'Neill, 1963):

$$R_k = U_{k,0} + U_{k,2} + rQ_{k,1}, \quad F_k = U_{k,0} - U_{k,2}$$
$$Z_k = U_{k,1} + (z + 1 + d)Q_{k,1}, \ P_k = 2Q_{k,1}, \ (k = 1, 2). \tag{9}$$

Such a substitution leads to simplification of eq. (1) in the sense that a particular equation is formulated for each of the unknown functions in eq. (9). Thus, we are left with a set of partial differential equations which have to be satisfied by $U_{k,0}$, $U_{k,1}$, $U_{k,2}$ and $Q_{k,1}$:

$$L_m[U_{k,m}] = 0, \quad L_1[Q_{k,1}] = 0,$$
$$(m = 0, 1, 2;\ k = 1, 2). \tag{10}$$

Here the operator L_m is defined as

$$L_m = \frac{\partial^2}{\partial r^2} + \frac{1}{r}\frac{\partial}{\partial r} + \frac{\partial^2}{\partial z^2} - \frac{m^2}{r^2}. \tag{11}$$

In the bipolar coordinates (6), (7) one can solve eqs (10), (11) by separation of variables. The general solution is represented as series of exponents multiplied by associated Legendre functions. The latter are conventionally expressed by the relation (cf. Arfken, 1985)

$$P_{n,m}(\xi) = \frac{1}{2^n n!}(1 - \xi^2)^{m/2}\frac{\mathrm{d}^{n+m}}{\mathrm{d}\xi^{n+m}}[(\xi^2 - 1)^n],$$
$$(n \geqslant m). \tag{12}$$

In the phase Ω_1 we obtain the following solutions:

$$U_{1,m} = \sqrt{\cosh x_1 - \cos x_2} \times \sum_{n=m}^{\infty} \left\{ A_{n,m} \frac{\sinh[\lambda_n(x_1 + c)]}{\sinh(\lambda_n c)} - B_{n,m} \frac{\sinh(\lambda_n x_1)}{\sinh(\lambda_n c)} \right\} P_{n,m}(\cos x_2) \quad (13)$$

$$Q_{1,1} = \frac{\sqrt{\cosh x_1 - \cos x_2}}{b} \times \sum_{n=1}^{\infty} \left\{ A_{n,3} \frac{\sinh[\lambda_n(x_1 + c)]}{\sinh(\lambda_n c)} - B_{n,3} \frac{\sinh(\lambda_n x_1)}{\sinh(\lambda_n c)} \right\} P_{n,1}(\cos x_2). \quad (14)$$

In the volume Ω_2, the results read

$$U_{2,m} = \sqrt{\cosh x_1 - \cos x_2} \sum_{n=m}^{\infty} \times a_{n,m} \exp(-\lambda_n x_1) P_{n,m}(\cos x_2) \quad (15)$$

$$Q_{2,1} = \frac{\sqrt{\cosh x_1 - \cos x_2}}{b} \times \sum_{n=1}^{\infty} a_{n,3} \exp(-\lambda_n x_1) P_{n,1}(\cos x_2). \quad (16)$$

Here $m = 0, 1, 2$, and the separation constant, λ_n, acquires discrete values

$$\lambda_n = n + \tfrac{1}{2}, \quad n = 0, 1, 2, \ldots . \quad (17)$$

The form of the series (15), (16) takes into account the fact that the region Ω_2 contains the pole $z = -(1 + d) - b$, where $x_1 = \infty$. As the solution should be finite, there are no terms $\exp(\lambda_n x_1)$ in eqs (15), (16).

Now, we encounter the problem of finding the unknown numerical coefficients in eqs (13)–(16). Connections between these coefficients can be established by utilising the boundary conditions and the equation of incompressibility, eq. (2). In cylindrical coordinates we transform eq. (2) in terms of the auxiliary functions from eq. (9):

$$\frac{\partial U_{k,0}}{\partial r} + \frac{\partial U_{k,2}}{\partial r} + \frac{2U_{k,2}}{r} + \frac{\partial U_{k,1}}{\partial z} + 3Q_{k,1} + r\frac{\partial Q_{k,1}}{\partial r} + (z + 1 + d)\frac{\partial Q_{k,1}}{\partial z} = 0, \quad (k = 1, 2). \quad (18)$$

3. BOUNDARY CONDITIONS

3.1. *Velocity*

First of all, we mention that the fluid is supposed to be at rest very far from the particle (with x_1 and x_2 simultaneously approaching zero). This condition is automatically fulfilled given the form of eqs (13)–(16).

There is no mass transfer across the flat liquid interface S_2. For that reason, the normal velocity components, v_{z1}, v_{z2}, on both sides of S_2, should vanish. In other words, $Z_1 = Z_2 = 0$ at $x_1 = 0$. From eqs (9), (13) and (15) it follows that

$$A_{n,1} = 0, \quad a_{n,1} = 0 \quad \text{for } n \geqslant 1. \quad (19)$$

Besides, let us mention that $U_{2,1} = 0$ in the whole phase Ω_2.

On the solid surface of the sphere the velocity is prescribed. Therefore, we specify its three components on S_1 by writing

$$R_1 = F_1 = 1 - \varepsilon - \varepsilon z, \quad Z_1 = \varepsilon r \text{ at } x_1 = -c \quad (20)$$

where ε distinguishes between translation along Oy-axis ($\varepsilon = 0$) and rotation around Ox-axis ($\varepsilon = 1$). The condition for Z_1 can be combined with eq. (9) and with the solutions in the phase 1, eqs (13), (14). We substitute r and z according to eq. (6), and make use of the identity

$$\frac{1}{\sqrt{\cosh c - \cos x_2}} = \sqrt{2} \times \sum_{n=0}^{\infty} P_{n,0}(\cos x_2) \exp(-\lambda_n c) \quad (21)$$

(see Jahnke *et al.*, 1960, Section 8), in order to express all terms in the resulting equation as infinite series of associated Legendre functions. This yields

$$\cosh c \sum_{n=1}^{\infty} B_{n,1} P_{n,1}(\cos x_2) - \sum_{n=1}^{\infty} B_{n,1} \cos x_2 P_{n,1}(\cos x_2) + \sinh c \sum_{n=1}^{\infty} B_{n,3} P_{n,1}(\cos x_2) = \varepsilon b \sqrt{2} \sum_{n=0}^{\infty} \exp(-\lambda_n c) \sin x_2 P_{n,0}(\cos x_2) \quad (22)$$

valid for arbitrary x_2 within the range $(0, \pi)$. Now some transformations are applied in eq. (22) so as to obtain sums which depend upon x_2 only through $P_{n,1}(\cos x_2)$. Since $P_{n,1}$ ($n = 1, 2, 3, \ldots$) represent a set of linearly independent functions, we equate the multiplying coefficients for each value of n and find

$$B_{n,3} = \frac{n-1}{2b\lambda_{n-1}} B_{n-1,1} - \frac{1+d}{b} B_{n,1} + \frac{n+2}{2b\lambda_{n+1}} B_{n+1,1} + \frac{\sqrt{2}}{2} \varepsilon \exp(-\lambda_n c) \left(\frac{1 + d + b}{\lambda_{n-1}} - \frac{1 + d - b}{\lambda_{n+1}} \right) \quad n \geqslant 1. \quad (23)$$

The relations

$$b = \sinh c; \quad 1 + d = \cosh c \quad (24)$$

have been used for the derivation.

It is evident from eq. (20) that $R_1 - F_1 = 0$ at $x_1 = -c$. Then, substitution with eqs (9), (13) and (14) gives

$$B_{n,2} = \frac{1}{4b\lambda_{n-1}} B_{n-1,1} - \frac{1}{4b\lambda_{n+1}} B_{n+1,1} - \frac{\sqrt{2}}{2} \varepsilon \exp(-\lambda_n c)\left(\frac{1+d+b}{\lambda_{n-1}} - \frac{1+d-b}{\lambda_{n+1}} \right) \quad n \geqslant 2. \tag{25}$$

The calculations are similar to those which led to eq. (23), and that is why only the final result is presented here.

From eq. (20) one has $R_1 + F_1 = 2(1 - \varepsilon - \varepsilon z)$ at $x_1 = -c$. In analogous manner, with eqs (9), (13) and (14) there follows:

$$B_{n,0} = -\frac{(n-1)n}{4b\lambda_{n-1}} B_{n-1,1} + \frac{(n+1)(n+2)}{4b\lambda_{n+1}} B_{n+1,1} + \sqrt{2}\exp(-\lambda_n c)\left[1 - \varepsilon - \varepsilon \times \left(\lambda_n b + \frac{1+d+\lambda_n b}{4\lambda_{n-1}\lambda_{n+1}} \right) \right] \quad n \geqslant 0. \tag{26}$$

The three eqs (23), (25) and (26) establish connections between $B_{n,3}$, $B_{n,2}$, $B_{n,0}$, and $B_{n,1}$. Below it will be shown that using the other boundary conditions on the surface S_2, as well as the equation of continuity, eq. (2), one can express the coefficients $A_{n,0}$, $A_{n,2}$ and $A_{n,3}$ explicitly in terms of $a_{n,0}$, $a_{n,2}$, $a_{n,3}$ and $B_{n,1}$.

At the fluid interface, S_2, the two tangential velocity components should acquire equal values from the sides of the two adjacent bulk phases, Ω_1 and Ω_2, i.e. $v_{r,1} = v_{r,2}$; $v_{\varphi,1} = v_{\varphi,2}$ for $x_1 = 0$. On the other hand, in cylindrical coordinates the condition for incompressibility, eq. (2), reads

$$\frac{\partial v_{r,k}}{\partial r} + \frac{1}{r} v_{r,k} + \frac{1}{r}\frac{\partial v_{\varphi,k}}{\partial \varphi} + \frac{\partial v_{z,k}}{\partial z} = 0, \quad k = 1, 2. \tag{27}$$

It can be applied in the limit $z \to -(1+d)$, $x_1 \to 0$. Thus, we obtain

$$\frac{\partial Z_1}{\partial z} = \frac{\partial Z_2}{\partial z} \quad \text{at } x_1 = 0. \tag{28}$$

After transformation of eq. (28) into bipolar coordinates, eqs (9), (13)–(16) are inserted there to produce the following result:

$$A_{n,3} = a_{n,3} + \frac{(n-1)B_{n-1,1}}{2\sinh(\lambda_{n-1}c)} - \frac{\lambda_n B_{n,1}}{\sinh(\lambda_n c)} + \frac{(n+2)B_{n+1,1}}{2\sinh(\lambda_{n+1}c)}, \quad n \geqslant 1. \tag{29}$$

It is convenient to use the conditions for continuity of tangential velocity on S_2 in the form

$$R_1 + F_1 = R_2 + F_2; \quad R_1 - F_1 = R_2 - F_2 \quad \text{at } x_1 = 0. \tag{30}$$

When the first relation (30) is combined with eqs (9), (13)–(16) and (29), one finds

$$A_{n,0} = a_{n,0} - \frac{(n-1)n}{4\sinh(\lambda_{n-1}c)} B_{n-1,1} + \frac{(n+1)(n+2)}{4\sinh(\lambda_{n+1}c)} B_{n+1,1}, \quad n \geqslant 0. \tag{31}$$

In much the same manner, the second eq. (30) yields

$$A_{n,2} = a_{n,2} + \frac{B_{n-1,1}}{4\sinh(\lambda_{n-1}c)} - \frac{B_{n+1,1}}{4\sinh(\lambda_{n+1}c)}, \quad n \geqslant 2. \tag{32}$$

Up to this point, we have the quantities $B_{n,3}$, $B_{n,2}$, $B_{n,0}$, $A_{n,3}$, $A_{n,0}$, and $A_{n,2}$ represented explicitly by means of $a_{n,0}$, $a_{n,2}$, $a_{n,3}$, and $B_{n,1}$, the latter remaining as unknowns. Hence, in order to determine all coefficients in the series (13)–(16) it is necessary to find another four sequences of equations connecting $a_{n,0}$, $a_{n,2}$, $a_{n,3}$, and $B_{n,1}$. Two of them come from the incompressibility in the phases Ω_1, Ω_2, and the other two are due to the stress conditions on the liquid interface S_2.

We now substitute eqs (15) and (16) into eq. (18) with $k = 2$, which gives the incompressibility in the bulk volume Ω_2. All terms are cast to the form of infinite sums containing one and the same functions of the two independent variables x_1, x_2. In particular, we encounter the functions

$$\exp(-\lambda_n x_1)\frac{1}{\sin x_2}[P_{n-1,0}(\cos x_2) - \cos x_2 P_{n,0}(\cos x_2)], \quad (n = 1, 2, 3, \ldots). \tag{33}$$

As the equation should hold for arbitrary x_1, x_2, the multiplying constant factors are obliged to satisfy the following relations for each value of n:

$$a_{n-1,0} - 2a_{n,0} + a_{n+1,0} - (n-1)(n-2)a_{n-1,2} + 2(n-1)(n+2)a_{n,2} - (n+2)(n+3)a_{n+1,2} + (n-1)a_{n-1,3} - 5a_{n,3} - (n+2)a_{n+1,3} = 0, \quad n \geqslant 1. \tag{34}$$

Similarly, we can treat the condition for incompressibility in the phase Ω_1. Solutions (13), (14) are inserted in (eq. 18) with $k = 1$. Again, the dependence upon x_1, x_2 is contained in series of linearly independent functions. However, in this case two different kinds of such functions appear—the first one is as in eq. (33), and the second kind reads

$$\exp(\lambda_n x_1)\frac{1}{\sin x_2}[P_{n-1,0}(\cos x_2) - \cos x_2 P_{n,0}(\cos x_2)], \quad (n = 1, 2, 3, \ldots).$$

For arbitrary x_1, x_2 the multiplying coefficients have to be equated separately. Therefore, we are left with two sequences of relations for $n = 1, 2, 3, \ldots$. On the other hand, the continuity equation has already been used once during the derivation of eq. (28). This is the reason why we are allowed to introduce only one

independent set of connections between the coefficients. Analogous lines of consideration can be found in the paper by Dean and O'Neill (1963, p. 19). Thus, from eq. (18) with $k = 1$ we write

$$\begin{aligned}
&\frac{b}{\sin(\lambda_{n-1}c)}[A_{n-1,0} + (n-1)A_{n-1,3} \\
&\quad - (n-2)(n-1)A_{n-1,2}] + \frac{b}{\sinh(\lambda_{n+1}c)} \\
&\quad \times [-A_{n+1,0} + (n+2)A_{n+1,3} \\
&\quad + (n+2)(n+3)A_{n+1,2}] \\
&\quad + \frac{\sinh(\lambda_n c)}{\sinh(\lambda_{n-1}c)}[-B_{n-1,0} - (n-1)B_{n-1,3} \\
&\quad + (n-2)(n-1)B_{n-1,2}] + 2B_{n,0} + 5B_{n,3} \\
&\quad - 2(n-1)(n+2)B_{n,2} + \frac{\sinh(\lambda_n c)}{\sinh(\lambda_{n+1}c)} \\
&\quad \times [-B_{n+1,0} + (n+2)B_{n+1,3} \\
&\quad + (n+2)(n+3)B_{n+1,2}] \\
&\quad - (n-1)\frac{\cosh(\lambda_n c)}{\sinh(\lambda_{n-1}c)}B_{n-1,1} \\
&\quad + (2n+1)\frac{\cosh(\lambda_n c)}{\sinh(\lambda_n c)} \\
&\quad \times B_{n,1} - (n+2)\frac{\cosh(\lambda_n c)}{\sinh(\lambda_{n+1}c)}B_{n+1,1} = 0.
\end{aligned}$$

Substitution with eqs (23), (25), (26), (29), (31) and (32) into the above equation yields

$$\begin{aligned}
&\frac{(n-1)\sinh(\lambda_n c)}{n\sinh(\lambda_{n-1}c)}\left(k_{n-1} - \frac{\lambda_{n-2}}{\lambda_{n-1}}k_n\right)B_{n-1,1} \\
&\quad + \left(\frac{n+1}{n}\frac{\lambda_{n+1}}{\lambda_n}k_{n+1} - \frac{5k_n}{n} - \frac{\lambda_{n-1}}{\lambda_n}k_{n-1}\right)B_{n,1} \\
&\quad + \frac{(n+2)\sinh(\lambda_n c)}{n\sinh(\lambda_{n+1}c)}\left(\frac{\lambda_{n+2}}{\lambda_{n+1}}k_n - k_{n+1}\right)B_{n+1,1} \\
&\quad + \frac{b}{n\sinh(\lambda_{n-1}c)}[(n-2)(n-1)a_{n-1,2} \\
&\quad - (n-1)a_{n-1,3} - a_{n-1,0}] + \frac{b}{n\sinh(\lambda_{n+1}c)} \\
&\quad \times [a_{n+1,0} - (n+2)a_{n+1,3} \\
&\quad - (n+2)(n+3)a_{n+1,2}] \\
&\quad = \frac{\sqrt{2}(1-\varepsilon)}{n\exp(\lambda_n c)}\left[2 - (1+d+b)\frac{\sinh(\lambda_n c)}{\sinh(\lambda_{n-1}c)}\right. \\
&\quad \left. - (1+d-b)\frac{\sinh(\lambda_n c)}{\sinh(\lambda_{n+1}c)}\right] + \frac{\sqrt{2}\varepsilon}{n\exp(\lambda_n c)} \\
&\quad \times \left[\frac{2(1+d)\lambda_n^2 + 2b\lambda_n}{\lambda_{n-1}\lambda_{n+1}} - \frac{\lambda_{n-1}\sinh(\lambda_n c)}{\lambda_n\sinh(\lambda_{n-1}c)}\right. \\
&\quad \left. - \frac{\lambda_{n+1}\sinh(\lambda_n c)}{\lambda_n\sinh(\lambda_{n+1}c)}\right] \qquad (35)
\end{aligned}$$

where $k_n = \lambda_n\coth(\lambda_n c) - (1+d)/b$. It can be verified that if the surface S_2 is tangentially immobile (which means zero velocity and pressure in the volume Ω_2), then eq. (35) for translation ($\varepsilon = 0$) coincides identically with eq. (23) from the work of O'Neill (1964).

3.2. *Tangential stress*

Let us now pay attention to the stress conditions imposed on the fluid boundary S_2. We shall take into account the intrinsic viscous behaviour of this interface, which is supposed to be Newtonian. Within the frames of the Boussinesq–Scriven theory, the constitutive relation for the two-dimensional stress tensor, $\mathbf{T}_{\mathrm{II}}$, on arbitrary surface, S, reads

$$\begin{aligned}
\mathbf{T}_{\mathrm{II}} &= \gamma\mathbf{U}_{\mathrm{II}} + \eta_d(\nabla_{\mathrm{II}}\cdot\mathbf{v})\mathbf{U}_{\mathrm{II}} + 2\eta_{\mathrm{sh}}[\mathbf{D} - \tfrac{1}{2}(\nabla_{\mathrm{II}}\cdot\mathbf{v})\mathbf{U}_{\mathrm{II}}] \\
&= [\gamma + (\eta_d - \eta_{\mathrm{sh}})(\nabla_{\mathrm{II}}\cdot\mathbf{v})]\mathbf{U}_{\mathrm{II}} + 2\eta_{\mathrm{sh}}\mathbf{D} \qquad (36)
\end{aligned}$$

(see Slattery, 1990). Here γ is the interfacial tension and η_d, η_{sh} represent the two independent surface viscosities corresponding to dilatation and shear, respectively. The velocity of the surface material points is denoted by $\mathbf{v}$, and ∇_{II} is the two-dimensional gradient operator, $\mathbf{U}_{\mathrm{II}}$ is the surface idemfactor, $\mathbf{D}$ is the rate-of-strain tensor on S:

$$\mathbf{D} = \tfrac{1}{2}\mathbf{U}_{\mathrm{II}}\cdot[(\nabla_{\mathrm{II}}\mathbf{v}) + (\nabla_{\mathrm{II}}\mathbf{v})^{\mathrm{T}}]\cdot\mathbf{U}_{\mathrm{II}}. \qquad (37)$$

The symbol $(\,)^{\mathrm{T}}$ means transposition. Besides, $\nabla_{\mathrm{II}}\cdot\mathbf{v} = \mathbf{U}_{\mathrm{II}}:\mathbf{D}$. In the two volume phases adjacent to S the bulk stress tensors, $\mathbf{T}_k$, obey the equations

$$\mathbf{T}_k = -p_k\mathbf{U} + \eta_k[(\nabla\mathbf{v}_k) + (\nabla\mathbf{v}_k)^{\mathrm{T}}], \quad k = 1, 2. \qquad (38)$$

Here $\mathbf{U}$ is the three-dimensional unit tensor. In all practical circumstances the surface mass density is very small owing to the extreme thinness of the interfacial transition zone (cf. Edwards *et al.*, 1991). Then, the balance of momentum transport at S reduces to the form

$$\nabla_{\mathrm{II}}\cdot\mathbf{T}_{\mathrm{II}} = \mathbf{n}\cdot(\mathbf{T}_2 - \mathbf{T}_1) \qquad (39)$$

where $\mathbf{n}$ represents the running unit normal to the surface (directed from phase 2 towards phase 1). $\mathbf{T}_1$ and $\mathbf{T}_2$ are taken on S. Equation (39) can be resolved into tangential and normal components with respect to S. The tangential projection reads

$$\begin{aligned}
\mathbf{n}\cdot(\mathbf{T}_2 - \mathbf{T}_1)\cdot\mathbf{U}_{\mathrm{II}} &= (\eta_d - \eta_{\mathrm{sh}})\nabla_{\mathrm{II}}(\nabla_{\mathrm{II}}\cdot\mathbf{v}) \\
&\quad + 2\eta_{\mathrm{sh}}(\nabla_{\mathrm{II}}\cdot\mathbf{D})\cdot\mathbf{D}_{\mathrm{II}} \qquad (40)
\end{aligned}$$

if γ, n_d and η_{sh} are constant. This assumption about the interfacial tension, γ, calls for additional discussion. Indeed, it is known that when suractants are present on a liquid phase boundary any surface motion accompanied with compression or expansion can cause local variations in the concentration of the adsorbed molecules. The change in γ is proportional to the relative dilatation (elastic behaviour) and, consequently, surface gradients of γ would appear (cf. Edwards *et al.*, 1991). In our considerations we discard $\nabla_{\mathrm{II}}\gamma$ in eq. (40), but still keep terms with dilatational viscosity. From a physical point of view, this situation may correspond to systems which contain

surfactants with bulk concentration above the critical micellization concentration (CMC). In such solutions surfactant aggregates (micelles) exist and usually they are capable of fast disintegration, thus providing a source of monomers very close to the surface. As the produced single molecules adsorb, they eliminate the interfacial tension gradients caused by the convective transport. The characteristic time of demicellisation for most common surfactants is quite short, typically of the order of milliseconds (cf. Hunter, 1987). Another possible case for which γ can be constant is that of small surface Peclet number (aV_*/D_s, where D_s denotes surface diffusivity)—see the extended discussion in the book of Edwards *et al.* (1991, Section 5.6). The motion is assumed to be so slow that the molecular surface diffusion is able to completely restore the uniform surfactant distribution along the phase boundary.

We apply eq. (40) for the liquid interface S_2 (Fig. 1), which is flat in zeroth-order approximation. The rate-of-strain tensor, $\mathbf{D}$, is expressed in cylindrical coordinates and sustituted into eq. (40). With account of eq. (3), we deduce the following result for the radial component of eq. (40):

$$\frac{\partial}{\partial z}(\beta R_2 - R_1) = (k+e)\frac{\partial}{\partial r}\left(\frac{\partial R_2}{\partial r} + \frac{R_2 - F_2}{r}\right) + \frac{e}{r}\left(\frac{\partial F_2}{\partial r} + \frac{F_2 - R_2}{r}\right). \tag{41}$$

Here dimensionless quantities have been introduced: β denotes the ratio of the two bulk dynamic viscosities of the phases, $\beta = \eta_2/\eta_1$, and

$$k = \frac{\eta_d}{a\eta_1}, \quad e = \frac{\eta_{\mathrm{sh}}}{a\eta_1} \tag{42}$$

represent dilatational and shear interfacial viscosity numbers, respectively. Now, eq. (41) is combined with eqs (9), (13)–(16), and with the connections between the coefficients, eqs. (23) (25), (26), (29), (31) and (32). Thus, one finds for $n \geqslant 1$

$$\begin{aligned}
&-\left[\beta + \coth(\lambda_{n-1}c) + \frac{2e}{b}\right]a_{n-1,0} + \frac{4e}{b}a_{n,0} \\
&+\left[\beta + \coth(\lambda_{n+1}c) - \frac{2e}{b}\right]a_{n+1,0} \\
&+(n-2)(n-1)[\beta + \coth(\lambda_{n-1}c)]a_{n-1,2} \\
&-(n+2)(n+3)[\beta + \coth(\lambda_{n+1}c)]a_{n+1,2} \\
&+(n-1)\left[\frac{k}{b} - \beta - \coth(\lambda_{n-1}c)\right]a_{n-1,3} \\
&+\left[\frac{k+4e}{b} - 2\lambda_n\beta - 2\lambda_n\coth(\lambda_n c)\right]a_{n,3} \\
&-(n+2)\left[\frac{k}{b} + \beta + \coth(\lambda_{n+1}c)\right]a_{n+1,3} \\
&+\frac{n-1}{\sinh(\lambda_{n-1}c)}\left(k_{n-1} - \frac{\lambda_n}{\lambda_{n-1}}k_n\right)B_{n-1,1} \\
&+\frac{1}{\sinh(\lambda_n c)}\left[2\lambda_n k_n - \frac{\lambda_{n-1}}{\lambda_n}nk_{n-1} - \frac{\lambda_{n+1}}{\lambda_n}\right. \\
&\left.\times(n+1)k_{n+1}\right]B_{n,1} \\
&+\frac{n+2}{\sinh(\lambda_{n+1}c)}\left(k_{n+1} - \frac{\lambda_n}{\lambda_{n+1}}k_n\right)B_{n+1,1} \\
&=\frac{\sqrt{2}(1-\varepsilon)}{\exp(\lambda_n c)}\left[\frac{1+d-b}{\sinh(\lambda_{n+1}c)} - \frac{1+d+b}{\sinh(\lambda_{n-1}c)}\right] \\
&\frac{\sqrt{2}\varepsilon}{\lambda_n\exp(\lambda_n c)}\left[\frac{\lambda_{n+1}}{\sinh(\lambda_{n+1}c)} - \frac{\lambda_{n-1}}{\sinh(\lambda_{n-1}c)}\right. \\
&\left.-\frac{2\lambda_n^2(1+d+\lambda_n b)}{\lambda_{n-1}\lambda_{n+1}\sinh(\lambda_n c)}\right].
\end{aligned} \tag{43}$$

In a similar way, we take the meridional component of the tangential stress balance (40). At $x_1 = 0$ (that is, on S_2), one has

$$\frac{\partial}{\partial z}(\beta F_2 - F_1) = \frac{k+e}{r}\left(\frac{\partial R_2}{\partial r} + \frac{R_2 - F_2}{r}\right) + e\frac{\partial}{\partial r}\left(\frac{\partial F_2}{\partial r} + \frac{F_2 - R_2}{r}\right). \tag{44}$$

Using eqs (9), (13)–(16), (23), (25), (26), (29), (31) and (32), it is obtained that

$$\begin{aligned}
&-(n-1)\frac{e}{b}a_{n-2,0} + \left[\beta + \coth(\lambda_{n-1}c) + \frac{2\lambda_{n-2}e}{b}\right] \\
&\times a_{n-1,0} + \frac{5e}{b}a_{n,0} - \left[\beta + \coth(\lambda_{n+1}c) + \frac{2\lambda_{n+2}e}{b}\right] \\
&\times a_{n+1,0} + (n+2)\frac{e}{b}a_{n+2,0} \\
&+(n-2)(n-1)[\beta + \coth(\lambda_{n-1}c)]a_{n-1,2} \\
&-(n+2)(n+3)[\beta + \coth(\lambda_{n+1}c)]a_{n+1,2} \\
&-(n-2)(n-1)\frac{e}{2b}a_{n-2,3} + (n-1)\frac{e}{b}a_{n-1,3} \\
&+\left[\frac{2k}{b} + (n^2+n+3)\frac{e}{b}\right]a_{n,3} - (n+2)\frac{e}{b}a_{n+1,3} \\
&-(n+2)(n+3)\frac{e}{2b}a_{n+2,3} \\
&+\frac{\lambda_{n-1}k_{n-1} - \lambda_{n+1}k_{n+1}}{4\lambda_n\sinh(\lambda_n c)}B_{n,1} = \frac{\sqrt{2}(1-\varepsilon)}{\exp(\lambda_n c)} \\
&\times\left[\frac{1+d+b}{\sinh(\lambda_{n-1}c)} - \frac{1+d-b}{\sinh(\lambda_{n+1}c)}\right] + \frac{\sqrt{2}\varepsilon}{\lambda_n\exp(\lambda_n c)} \\
&\times\left\{\frac{1+d-b}{\sinh(\lambda_{n+1}c)}[\lambda_{n+2}(1+d) + 2b\lambda_{n+1}^2]\right. \\
&\left.-\frac{1+d+b}{\sinh(\lambda_{n-1}c)}[\lambda_{n-2}(1+d) + 2b\lambda_{n-1}^2]\right\}, \quad n \geqslant 1.
\end{aligned} \tag{45}$$

Now, we dispose of four independent sequences of equations for the coefficients $a_{n,0}$ ($n = 0, 1, 2, \dots$), $a_{n,2}$ ($n = 2, 3, 4, \dots$), $a_{n,3}$ ($n = 1, 2, 3, \dots$), and $B_{n,1}$ ($n = 1, 2, 3, \dots$). These are the sets (34), (35), (43) and (45), which can be solved numerically after being cut at a certain large value of n. Further, by means of eqs (23), (25), (26), (29), (31) and (32) one determines the rest of the coefficients in the series (13)–(16). This completes the solution of the problem because the velocity and pressure distributions can then readily be found through eq. (9), implementing the summation in eqs (13)–(16) at any point of the fluid domain. All constant coefficients necessarily converge to zero with increasing n.

Below we consider the balance of normal stresses on the liquid interface S_2. It turns out that the analysis will give us the opportunity to calculate the first-order perturbation in the shape of S_2.

3.3. *Normal stress*

We take normal projection of eq. (39), which is valid on a surface of arbitrary shape.

$$(\mathbf{nn}):(\mathbf{T}_2 - \mathbf{T}_1) = \mathbf{b}:\mathbf{T}_{\mathrm{II}} = \mathbf{2}H\gamma + 2\eta_{\mathrm{sh}}(\mathbf{b} - 2H\mathbf{U}_{\mathrm{II}}):(\nabla_{\mathrm{II}}\mathbf{v}) + 2H(\eta_d + \eta_{\mathrm{sh}})(\nabla_{\mathrm{II}}\cdot\mathbf{v}). \tag{46}$$

Here $\mathbf{b}$ is the tensor of curvature:

$$\mathbf{b} = -\nabla_{\mathrm{II}}\mathbf{n}; \quad 2H = \mathbf{b}:\mathbf{U}_{\mathrm{II}}. \tag{47}$$

The scalar H is called mean curvature. If the capillary number is a small parameter,

$$Ca \equiv \frac{\eta_1 V_*}{\gamma} \ll 1 \tag{48}$$

then the phase boundary S_2 is disturbed only slightly by the motion, as at sufficiently low velocity the viscous drag is much smaller than the interfacial tension, γ. One may use the approximation

$$2H \approx \nabla_{\mathrm{II}}^2\zeta \tag{49}$$

where $\zeta(r, \varphi)$ is the local deviation of S_2 from planarity. In such circumstances the equation which describes the shape of S_2 can be represented in the form

$$z = -(1+d) + \frac{1}{a}\zeta(r,\varphi) = -(1+d) + Ca\,L(r)\sin\varphi. \tag{50}$$

Here $L(r)$ is unknown function to be sought for. We turn to dimensionless variables in eq. (46) and it becomes evident that, up to leading order in Ca, the terms containing surface viscosities may be neglected. Hence, from eqs (46) and (49), one obtains

$$P_1 - 2\frac{\partial Z_1}{\partial z} - \beta\left(P_2 - 2\frac{\partial Z_2}{\partial z}\right) = \frac{\mathrm{d}^2L}{\mathrm{d}r^2} + \frac{1}{r}\frac{\mathrm{d}L}{\mathrm{d}r} - \frac{L}{r^2} \tag{51}$$

on S_2. For the functions on the left-hand side of (51) we shall use the results which refer to perfectly flat interface (i.e., the zeroth-order approximation). In view of eq. (9), taking also into account that $U_{2,1} = 0$ in the whole phase Ω_2, and moreover, that $\partial Z_1/\partial z = \partial Z_2/\partial z$ at $x_1 = 0$, eq. (51) is transformed to read

$$\frac{\mathrm{d}^2L}{\mathrm{d}r^2} + \frac{1}{r}\frac{\mathrm{d}L}{\mathrm{d}r} - \frac{L}{r^2} = 2(Q_{1,1} - Q_{2,1}) \quad \text{at } x_1 = 0. \tag{52}$$

As suggested by the expressions (14), (16) for $Q_{1,1}$ and $Q_{2,1}$, a solution of (52) can be found in the following form:

$$L = \sqrt{1-\cos x_2}\sum_{n=1}^{\infty} L_n P_n(\cos x_2). \tag{53}$$

We insert (eqs 53), (14) and (16) into (52), which yields a set of relations for the coefficients L_n:

$$-(n-2)(n-1)L_{n-2} + 4(n-1)nL_{n-1} - 6n(n+1)L_n + 4(n+1)(n+2)L_{n+1} - (n+2)(n+3)L_{n+2} = 8b(A_{3,n} - a_{3,n}) \quad n \geqslant 1. \tag{54}$$

The latter can be solved numerically as a linear system, if cut at a given n.

4. DRAG AND TORQUE

Let us consider now the force, $\mathbf{F}$, and the torque, $\mathbf{M}$, exerted on the spherical solid particle during its stationary motion. The surface S_1 (Fig. 1) is exposed to stresses from the surrounding fluid. As demonstrated by Happel and Brenner (1965), one may determine $\mathbf{F}$ and $\mathbf{M}$ through integration of those stresses over the closed surface of the body:

$$F = \int_{S_1} \mathbf{n}_1\cdot\mathbf{T}_1\,\mathrm{d}S_1 \tag{55}$$

$$\mathbf{M} = \int_{S_1} \mathbf{r}_1\times(\mathbf{n}_1\cdot\mathbf{T}_1)\,\mathrm{d}S_1. \tag{56}$$

Here $\mathbf{T}_1$ is the bulk stress tensor in the phase Ω_1, taken on S_1 [cf. eq. (38)]. The running unit normal to S_1 is denoted by $\mathbf{n}_1$ (it is directed outwards), and $\mathbf{r}_1$ is the position vector of the surface points. In our particular system the solutions for the velocity and pressure are represented by the expressions (3), (4), which are valid both for translation and for rotation. Then, from eqs. (55) and (56) with the help of eqs (3), (4) and (38), one obtains the following Cartesian components of $\mathbf{F}$ and $\mathbf{M}$:

$$F_x = 0, \quad F_y = -f6\pi\eta_1 a V_*, \quad F_z = 0 \tag{57}$$

$$M_x = -m8\pi\eta_1 a^2 V_*, \quad M_y = 0, \quad M_z = 0. \tag{58}$$

For the specific symmetry only the force F_y and the torque M_x are non-zero. In (57) and (58) we have introduced dimensionless drag and torque coefficients, f and m, which are given by explicit relations in

terms of the functions R_1, F_1, Z_1, and P_1 at $x_1 = -c$:

$$f = \frac{1}{6}\int_0^\pi \left\{ P_1 \sin^2\theta - \left[\sin\theta \frac{\partial}{\partial r}(R_1 + F_1) + \cos\theta \frac{\partial}{\partial z}(R_1 + F_1) \right] \sin\theta - \left(\cos\theta \frac{\partial Z_1}{\partial r} - \sin\theta \frac{\partial Z_1}{\partial z} \right) \sin\theta - Z_1 \cos\theta \right\} d\theta \quad (59)$$

$$m = \frac{1}{8}\int_0^\pi \left\{ \left(\sin\theta \frac{\partial F_1}{\partial z} + Z_1 \right) \cos^2\theta - \left(\frac{\partial R_1}{\partial z} + \frac{\partial Z_1}{\partial r} \right) \times (\sin^2\theta - \cos^2\theta) \sin\theta - \left(3\frac{\partial Z_1}{\partial z} - \frac{\partial F_1}{\partial r} - \frac{\partial R_1}{\partial r} \right) \times \cos\theta \sin^2\theta \right\} d\theta \quad (60)$$

Here θ is the polar angle; the integration is carried out along the surface S_1, where $r = \sin\theta$, $z = \cos\theta$. We chose to scale the drag force F_y in eq. (57) using the Stokes (1851) result for a rigid spherical particle translating with a constant velocity in an unbounded incompressible viscous liquid. In the latter case $f = 1, m = 0$, according to our notation [cf. eqs (57) and (58)]. Similarly, the torque M_x in eq. (58) is scaled with the Kirchhoff formula for steady rotation of a sphere in an unbounded fluid (see Lamb, 1945), then $f = 0, m = 1$. If the particle moves (translates or rotates) in the vicinity of the flat interface S_2 (Fig. 1), neither f nor m will be zero, and they can strongly deviate from unity. Below it will be shown that far away from S_2 the correct limiting values of f and m are approached.

In order to transform the right-hand sides of eqs (59), (60) we substitute with the auxiliary functions from eq. (9), and with the final solutions eqs (13), (14). The boundary conditions for the three velocity components on the solid surface S_1 are also taken into account. Thus, we arrive at the following expressions:

$$f = \frac{\sqrt{2}b}{3}\sum_{n=0}^{\infty} \left\{ [B_{n,0} + n(n+1)B_{n,3}] \frac{1}{\sinh(\lambda_n c)} - [A_{n,0} + n(n+1)A_{n,3}] \frac{\exp(-\lambda_n c)}{\sinh(\lambda_n c)} \right\} \quad (61)$$

$$m = \frac{\varepsilon}{3} + \frac{\sqrt{2}b^2}{4}\sum_{n=1}^{\infty} \left\{ \left(B_{n,1} + \frac{1+d}{b} B_{n,3} \right) \times \left[\coth(\lambda_n c) + \frac{1}{3} \right] - \frac{1+d}{b} \frac{A_{n,3}}{\sinh(\lambda_n c)} \right\} \frac{n(n+1)}{\exp(\lambda_n c)} + \frac{\sqrt{2}b}{4}\sum_{n=0}^{\infty} \left\{ B_{n,0} \left[\coth(\lambda_n c) + \frac{1}{3} \right] - \frac{A_{n,0}}{\sinh(\lambda_n c)} \right\} \frac{1+d-2b\lambda_n}{\exp(\lambda_n c)}. \quad (62)$$

After having determined the numerical coefficients in the series (13) and (14) up to a cetain large value of n, it is straightforward to carry out the summation in eqs (61) and (62). Thus, one can calculate f and m either for translation or for rotation. Let us emphasize that eqs (57)–(62) hold in both cases.

Any sufficiently slow motion can be represented as a superposition of elementary translations and rotations, since the governing equations and the boundary conditions are linear if the Reynolds and the capillary numbers vanish. We shall discuss in more details the realistic situation when a solid sphere, S_1, which is close to a large fluid interface, S_2, experiences an external force due to gravity, directed along the Oy-axis (Fig. 1). In steady-state conditions, the particle translates parallel to the flat surface with constant velocity V_c, and rotates around the Ox-axis with angular velocity ω_c. The buoyancy force is counterbalanced by the viscous friction:

$$\nabla\rho\tfrac{4}{3}\pi a^3 g = f_{\text{trans}} 6\pi\eta_1 a V_c + f_{\text{rot}} 6\pi\eta_1 a^2 \omega_c. \quad (63)$$

Here $\Delta\rho$ is the difference between the densities of the particle and the medium (phase Ω_1), g is the gravity acceleration. The two drag coefficients, f_{trans} and f_{rot}, quantify the respectively forces which emerge because of the translation and rotation (cf. eq. (57)), note that $V^* = a\omega_c$ for rotation). Similar arguments lead to the balance of torques in the form

$$0 = m_{\text{trans}} 8\pi\eta_1 a^2 V_c + m_{\text{rot}} 8\pi\eta_1 a^3 \omega_c. \quad (64)$$

The net torque should be zero, m_{trans} and m_{rot} refer to the corresponding elementary motions [cf. eq. (58)]. For a rigid sphere which moves under the action of buoyancy in an unbounded liquid the Stokes law is applicable:

$$\nabla\rho\tfrac{4}{3}\pi a^3 g = 6\pi\eta_1 a V_{\text{Stokes}} \quad (65)$$

with V_{Stokes} being the stationary velocity in this case. Combining eqs. (63)–(65), one derives

$$\frac{V_c}{V_{\text{Stokes}}} = -\frac{m_{\text{rot}}}{f_{\text{rot}} m_{\text{trans}} - f_{\text{trans}} m_{\text{rot}}} \quad (66)$$

$$\frac{a\omega_c}{V_{\text{Stokes}}} = \frac{m_{\text{trans}}}{f_{\text{rot}} m_{\text{trans}} - f_{\text{trans}} m_{\text{rot}}}. \quad (67)$$

The latter expressions allow us to calculate how much the steady velocities change due to the presence of the wall.

5. NUMERICAL RESULTS AND DISCUSSION

In this section we investigate the influence of the surface viscosity of the liquid-phase boundary S_2 upon the flow properties, drag and torque, at different distances of particle-wall separation, d (Fig. 1). The computations have been carried out according to the following scheme: First, we solve the linear set of eqs (34), (35), (43) and (45), for the coefficients $a_{n,0}(n \geqslant 0)$, $a_{n,2}(n \geqslant 2)$, $a_{n,3}(n \geqslant 1)$, and $B_{n,1}(n \geqslant 1)$. The Gauss–Seidel method is convenient for this system, which is predominantly diagonal. The adopted maximum value of n, at which the equations are cut, is connected with d. In general, at large d (of the order of 1) $n = 100$ suffices, whereas for $d \sim 0.001$

much more terms have to be taken, we use n up to 10,000.

Second, we substitute into eqs (23), (25), (26), (29), (31) and (32) to determine $B_{n,3}(n \geqslant 1)$, $B_{n,2}(n \geqslant 2)$, $B_{n,0}(n \geqslant 0)$, $A_{n,3}(n \geqslant 1)$, $A_{n,0}(n \geqslant 0)$, and $A_{n,2}(n \geqslant 2)$. Having found all coefficients in the series (13)–(16), we perform the summations and obtain the three velocity components and the pressure at each point of the flow domain in the phases Ω_1 and Ω_2 [cf. eqs (3), (4) and (9)]. In order to calculate the surface deformation, the linear set (54) is solved for the unknown constants $L_n(n \geqslant 1)$ which are after that inserted into eqs (53) and (50). The latter expression gives us the perturbed shape of S_2. The drag and torque coefficients, f and m, are determined by means of the explicit formulae (61), (62).

In Fig. 2, the velocity vector field is presented for the case of translation, with non-viscous interface

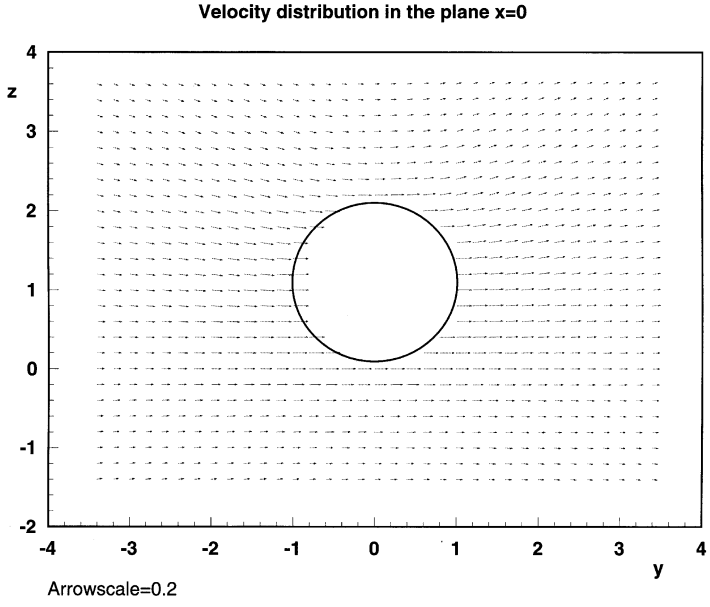

Fig. 2. Vetor plot of velocity in the plane $x = 0$. The liquid interface, located at $z = 0$, is non-viscous ($k = e = 0$); $\beta = \eta_2/\eta_1 = 0.907$. The particle translates at $d = 0.1$.

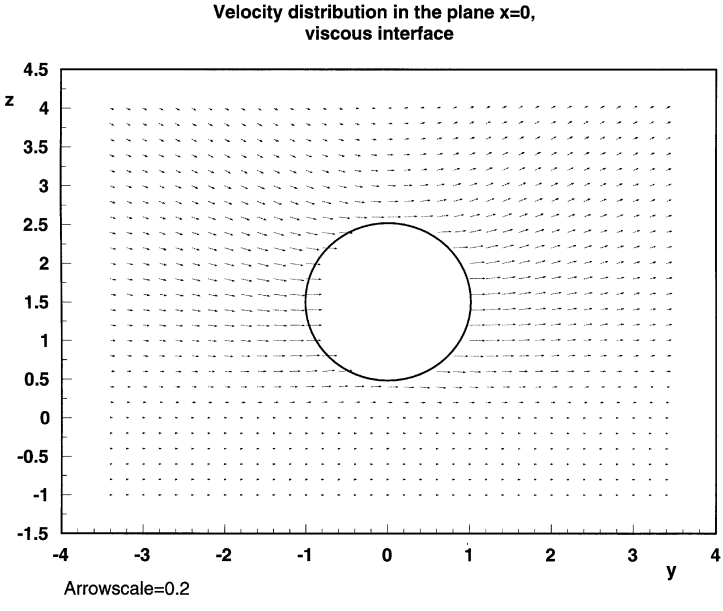

Fig. 3. Vector plot of velocity in the plane $x = 0$. The liquid interface, located at $z = 0$, is viscous ($k = e = 100$); $\beta = \eta_2/\eta_1 = 0.907$. The particle translates at $d = 0.5$.

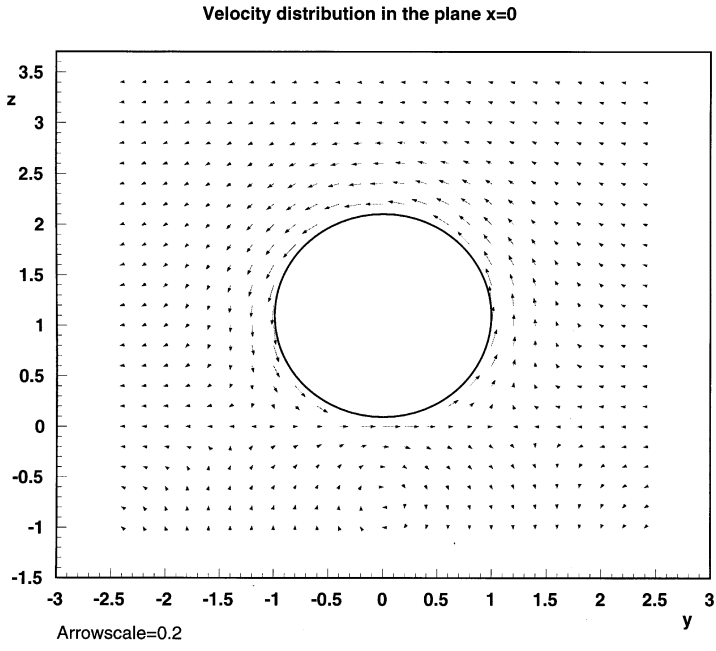

Fig. 4. Vector plot of velocity in the plane $x = 0$. The liquid interface, located at $z = 0$, is non-viscous ($k = e = 0$); $\beta = \eta_2/\eta_1 = 0.907$. The particle rotates at $d = 0.1$. The arrow heads are not drawn to scale, but have equal size.

S_2[$k = e = 0$, cf. eq. (42)]. S_2 is positioned at $z = 0$ and d is 0.1. One can see that the influence of the particle motion is far reaching, it extends to distances of the order of several sphere diameters. In addition, velocity of considerable magnitude is observed in the lower phase, Ω_2. Comparison can be made with the flow when the surface S_2 is viscous. The latter situation is illustrated in Fig. 3 for $k = e = 100$, $d = 0.5$. We assume equal dilatation and shear viscosities because this is so in most systems of practical importance (cf. Edwards *et al.*, 1991). Figure 3 shows that the fluid in the bulk Ω_2 is nearly at rest. Moreover, the velocity in the continuous phase Ω_1 turns out to decay faster as receding from the particle (compare with Fig. 2). It should be mentioned that for common low molecular weight surfactants the interfacial viscosity is between 10^{-4} and 1 sp (surface poise = g/s)—see Edwards *et al.* (1991). On the other hand, for proteins η_d and η_{sh} can range from 10 up to 10^3–10^4 sp (cf. Graham and Phillips, 1980a, b). With micron-sized particles, $a \sim 10^{-4}$ cm, eqs (42) provide an estimate $k \sim e > 10^2$, if $\eta_1 \sim 0.01$ g/(cm s). In general, the behaviour of the viscous surface at $k - e > 10^2$ is very close to that of a solid wall, as can be inferred from Fig. 3. Further numerical results described below support such a conclusion.

In Fig. 4 we plot the velocity distribution for the case of rotation, when the interface S_2 is non-viscous and $d = 0.1$. In contrast to translation, now the velocity is appreciable only in a close vicinity of the particle. The influence of the motion upon the fluid in the lower phase Ω_2 is minor. Nevertheless, it is interesting to note that a vortex exists in the bulk of Ω_2.

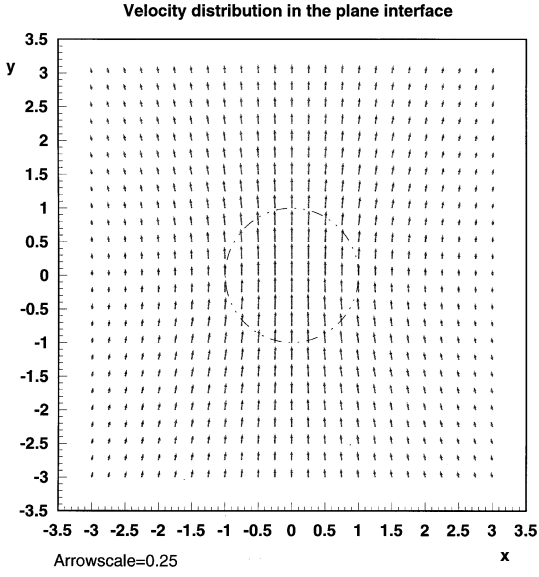

Fig. 5. Vector plot of velocity at the liquid-phase boundary, which is non-viscous ($k = e = 0$); $\beta = \eta_2/\eta_1 = 0.907$. The particle translates at $d = 0.1$ above the plane.

The coordinates of its centre in Fig. 4 are $x = 0$, $y = 0$, $z \approx -0.7$.

Figure 5 shows the velocity on a non-viscous surface S_2, as induced by translation of the sphere situated at a distance $d = 0.1$ above the plane. It is confirmed that the motion extends to a relatively large region, see also Fig. 2. Different is the case of rotation, which becomes evident from Fig. 6. Far away from

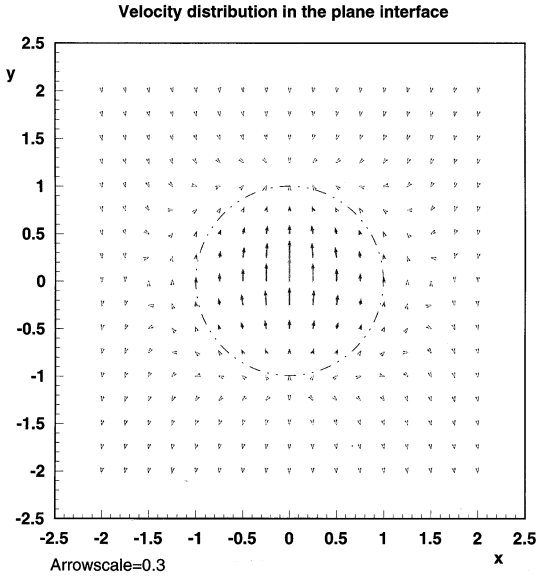

Fig. 6. Vector plot of velocity at the liquid-phase boundary, which is non-viscous ($k = e = 0$); $\beta = \eta_2/\eta_1 = 0.907$. The particle rotates at $d = 0.1$ above the plane. The arrow heads are not drawn to scale, but have equal size.

the particle we see the existence of very small velocity directed towards negative y.

The pressure distribution calculated for translation, with $k = e = 0$ and $d = 0.5$, is presented in Fig. 7 as a contour plot. In accord with the expectations, the pressure is positive in front of the particle (upstream), and is negative behind it (downstream), $p_i = 0$ at infinity ($i = 1, 2$). The pressure changes in the phase Ω_2 are much weaker than those inside Ω_1. This is a consequence from the fact that the fluid in Ω_2 moves tangentially, being dragged by the surface. In contrast, for rotation (Fig. 8) higher pressure develops in Ω_2, it is comparable with that above the non-viscous interface. The pattern of the liquid motion is more complicated in the latter case (Fig. 4). The impact of the viscous properties of S_2 on the pressure distribution is illustrated in Figs 9 and 10. Both for translation and for rotation we observe that a moderate surface viscosity ($k = e = 10$) reduces the pressure in the lower phase substantially. Particularly pronounced is the effect for rotation—compare Figs 10 and 8. The pressure in the region Ω_1 is influenced as well. It increases close to the sphere when the interface S_2 becomes viscous.

Figures 11 and 12 show the pressure within the liquid surface S_2, taken from the side of the upper phase Ω_1. The two pictures correspond to translation, $d = 0.1$. Higher values of the pressure are found with $k = e = 10$, compared to the case without surface viscosity. The same trend can be extracted also from Figs 7–10.

Computed deformations of the plane interface S_2 (non-viscous), due to translation and rotation of the spherical particle, are drawn in Figs 13 and 14. It is evident that for rotation the peaks are sharper, and

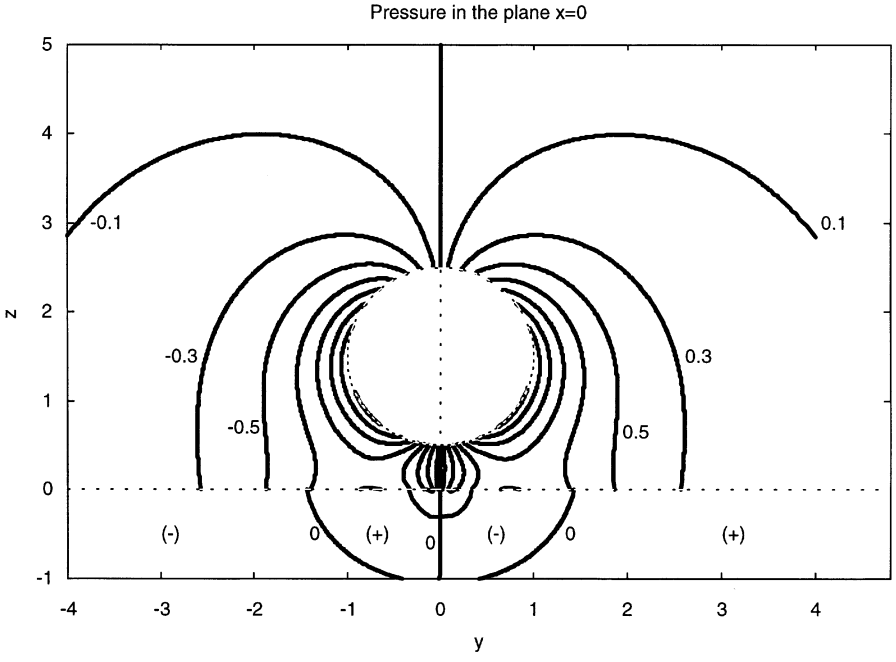

Fig. 7. Contour plot of the pressure in the plane $x = 0$. The liquid interface, located at $z = 0$, is non-viscous ($k = e = 0$); $\beta = \eta_2/\eta_1 = 0.907$. The particle translates at $d = 0.5$. Contours are drawn at levels 0, 0.1, 0.3, 0.5, 0.7, 0.9, 1.1, 1.3, and 1.5, positive and negative.

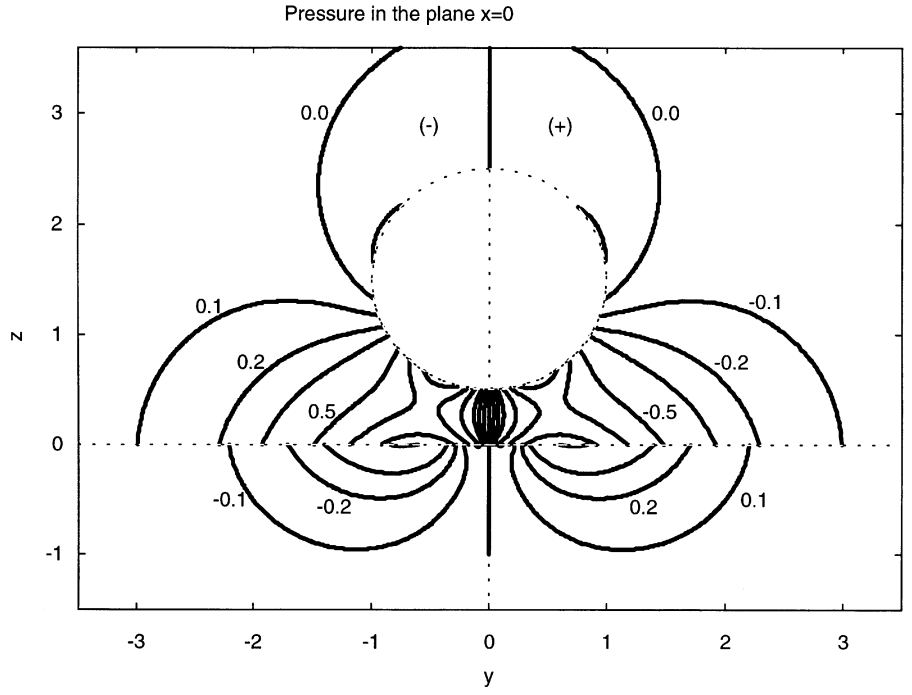

Fig. 8. Contour plot of the pressure in the plane $x = 0$. The liquid interface, located at $z = 0$, is non-viscous ($k = e = 0$); $\beta = \eta_2/\eta_1 = 0.907$. The particle rotates at $d = 0.5$. Contours are drawn at levels 0, 0.1, 0.2, 0.3, 0.5, 0.7, and 0.9, positive and negative.

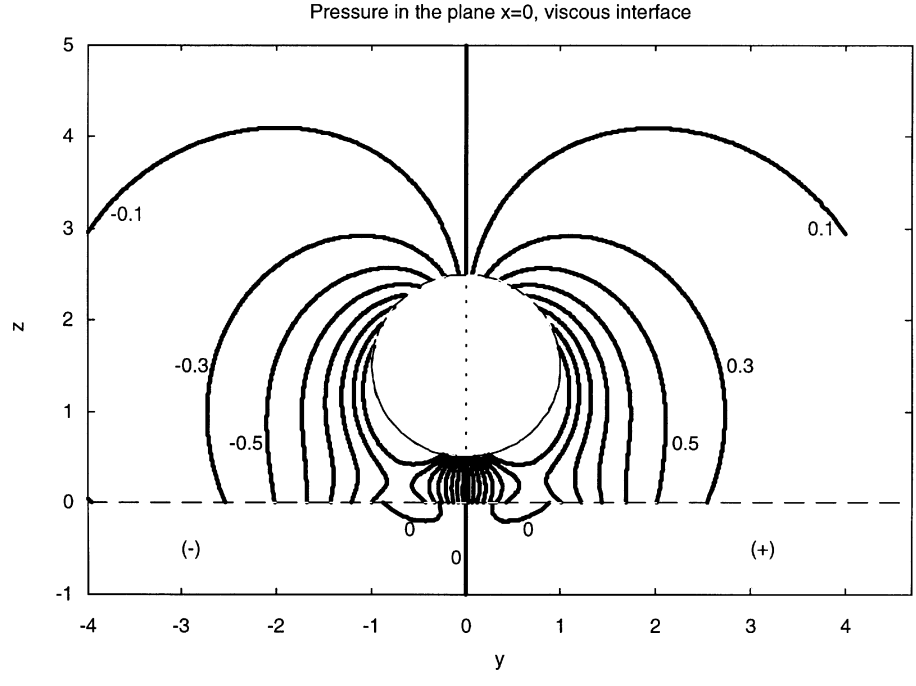

Fig. 9. Contour plot of the pressure in the plane $x = 0$. The liquid interface, located at $z = 0$, is viscous ($k = e = 10$); $\beta = \eta_2/\eta_1 = 0.907$. The particle translates at $d = 0.5$. Contours are drawn at levels 0, 0.1, 0.3, 0.5, 0.7, 0.9, 1.1, 1.3, and 1.5, positive and negative.

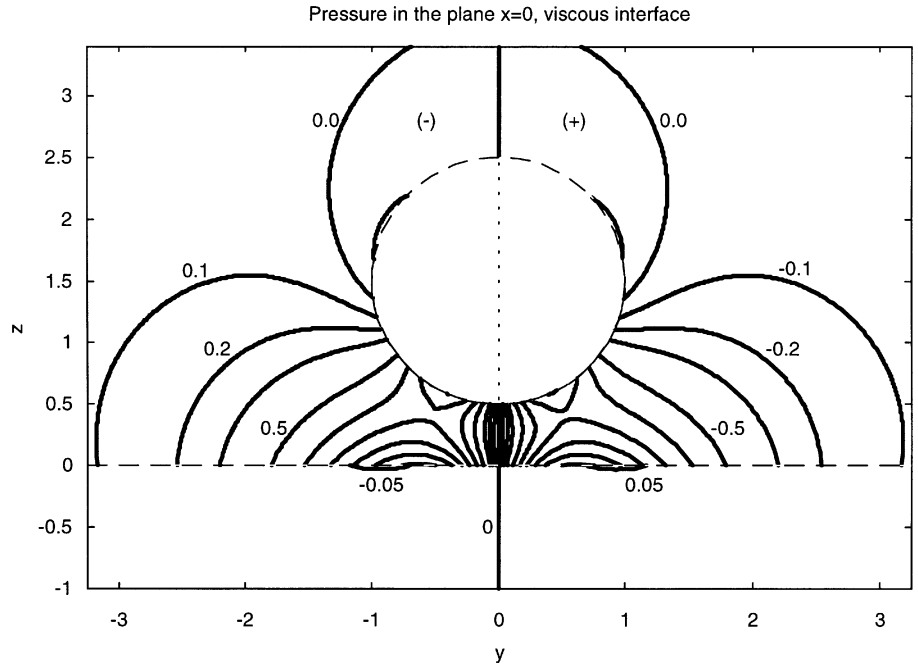

Fig. 10. Contour plot of the pressure in the plane $x = 0$. The liquid interface, located at $z = 0$, is viscous ($k = e = 10$); $\beta = \eta_2/\eta_1 = 0.907$. The particle rotates at $d = 0.5$. Contours are drawn at levels 0, 0.1, 0.2, 0.3, 0.5, 0.7, 0.9, 1.1, and 1.3, positive and negative.

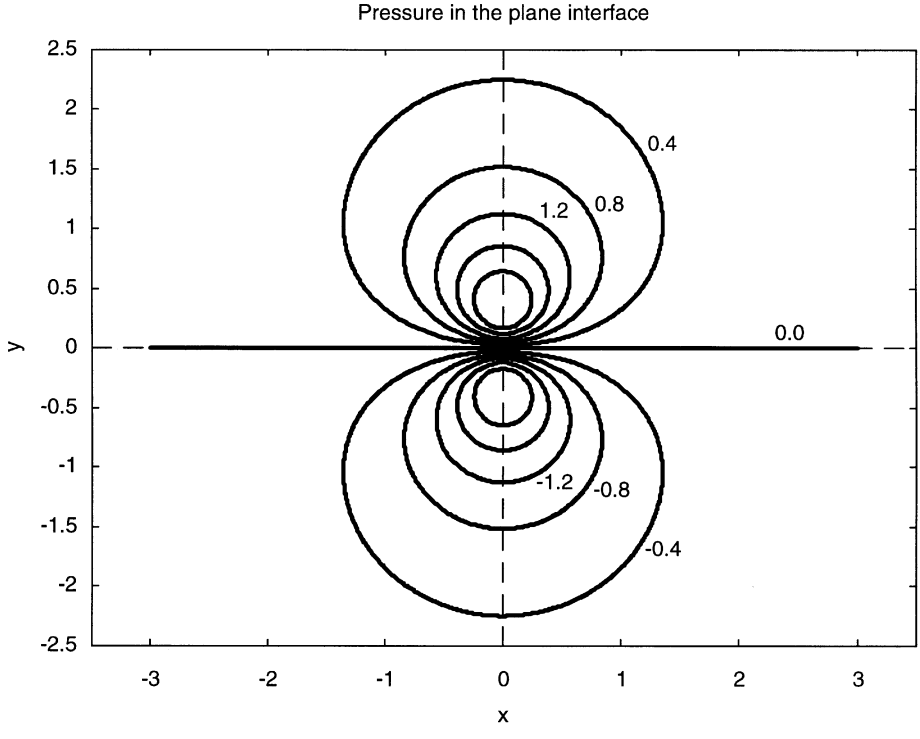

Fig. 11. Contour plot of the pressure at the liquid-phase boundary, which is non-viscous ($k = e = 0$); $\beta = \eta_2/\eta_1 = 0.907$. The particle translates at $d = 0.1$ above the plane. Contours are drawn at levels 0, 0.4, 0.8, 1.2, 1.6, and 2.0, positive and negative.

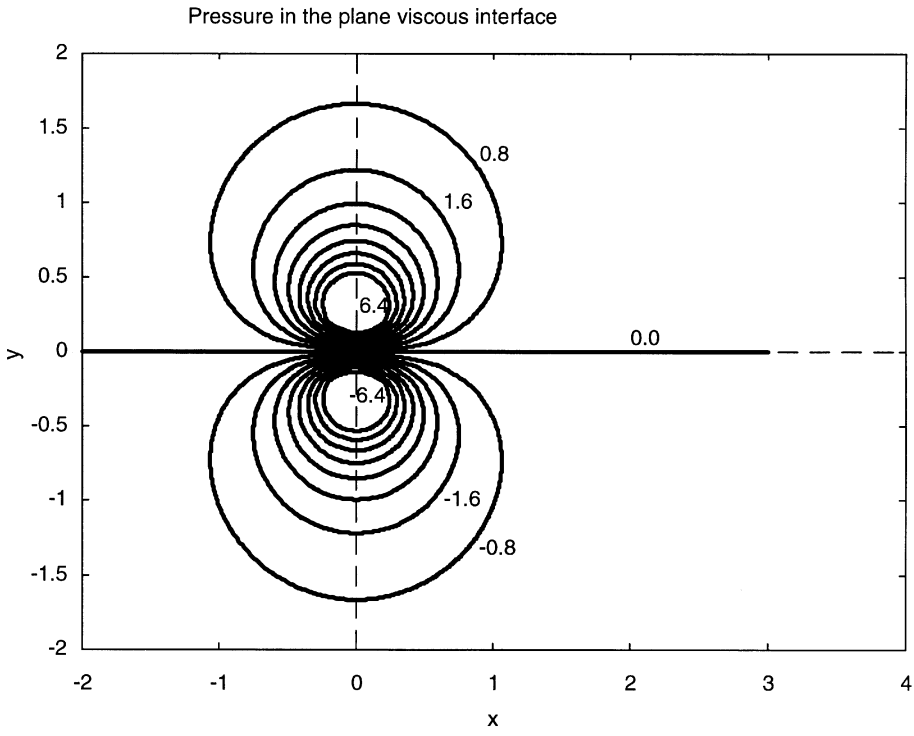

Fig. 12. Contour plot of the pressure at the liquid-phase boundary, which is viscous ($k = e = 10$); $\beta = \eta_2/\eta_1 = 0.907$. The particle translates at $d = 0.1$ above the plane. Contours are drawn at levels 0, 0.8, 1.6, 2.4, 3.2, 4.0, 4.8, 5.6, and 6.4, positive and negative.

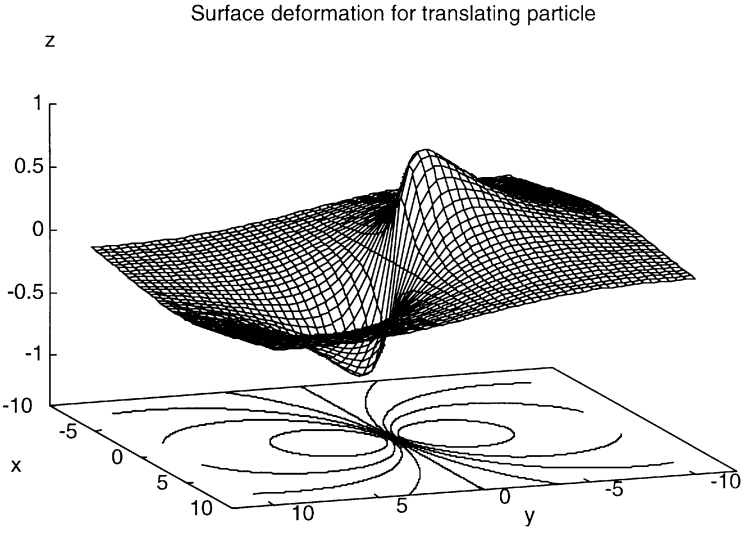

Fig. 13. Deformation of the liquid-phase boundary, which is non-viscous ($k = e = 0$); $\beta = \eta_2/\eta_1 = 0.907$. The particle translates at $d = 0.1$ above it. Note that the positive y-axis is directed to the left.

the magnitude of the deviation from planarity is higher. The dimensionless quantity plotted on the vertical axis is $L(r)\sin\varphi$, cf. eq. (41). Since the capillary number Ca is very small, one has $\zeta/a \ll 1$.

We investigate in more detail the behaviour of the drag and torque coefficients, f and m, at different conditions. Figure 15(a) presents the drag coefficient for translation, as a function of the particle–wall

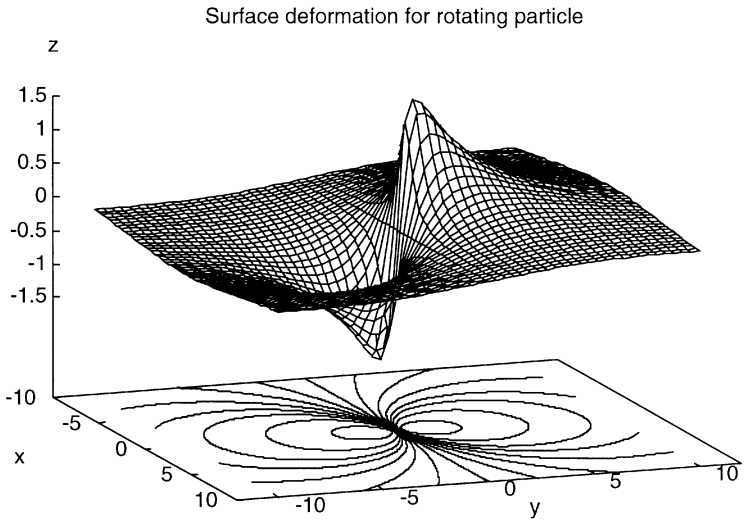

Fig. 14. Deformation of the liquid-phase boundary, which is non-viscous ($(k = e = 0)$; $\beta = \eta_2/\eta_1 = 0.907$. The particle rotates at $d = 0.1$ above it.

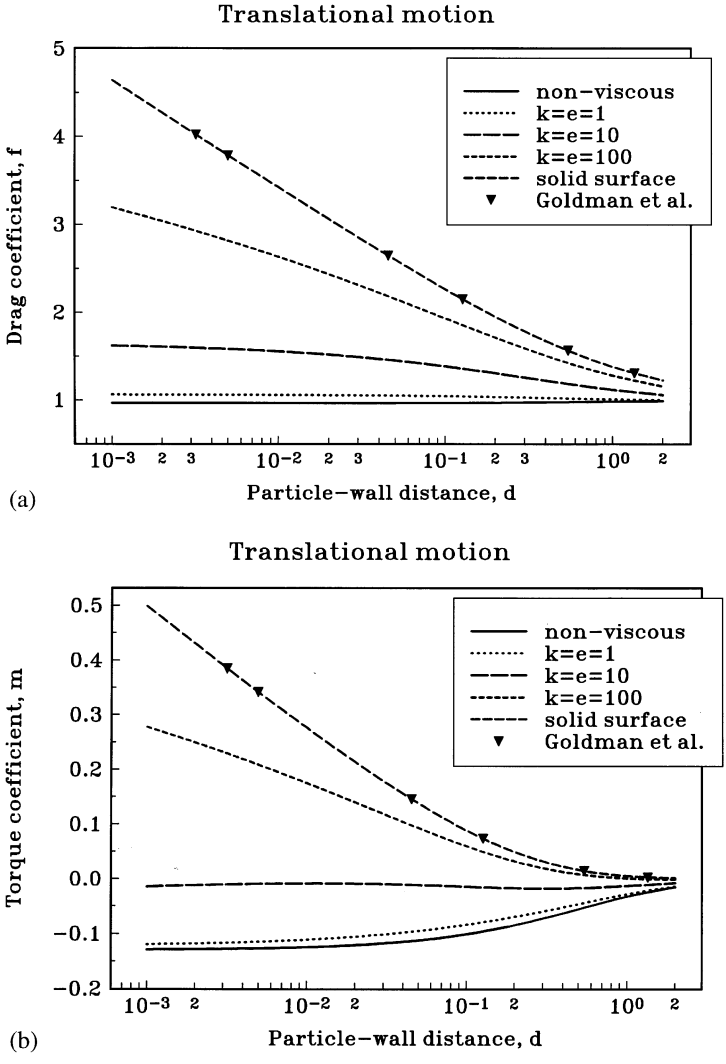

Fig. 15. (a) Dimensionless drag coefficient for translation, as a function of the particle–wall distance; (b) dimensionless torque coefficient for translation, as a function of the particle–wall distance.

separation distance. As can be anticipated, with decreasing d the drag force increases if S_2 possesses surface viscosity. At very large d all curves approach the value $f = 1$, which refers to motion in an unbounded liquid. The higher the surface viscosity, the greater the drag, with the limiting case being a solid wall. For the latter case we compare the results from our calculations with those of Goldman *et al.* (1967), and the full agreement is confirmed. When the interface is non-viscous, f is slightly below 1, which is explained by the circumstance that the bulk viscosity in the phase Ω_2 is assumed to be a bit lower than $\eta_1 : \beta = 0.907$. This corresponds, for example, to aqueous medium Ω_1, and the phase Ω_2 composed of *n*-decane, at 20°C.

The torque coefficient for translation, Fig. 15(b), generally exhibits the same trends with changing d and the surface viscosity. m approaches zero at $d \gg 1$, as it should be. In general, the values of the torque coefficient are roughly one order of magnitude smaller than f, with all conditions being the same. With low or zero interfacial viscosity m is negative, as the friction from the side of Ω_2 is smaller than that in Ω_1 above the particle. In other words, the induced moment is directed towards the positive x-axis. Figure 16 shows the respective dependencies for rotational motion. Appreciable drag force is observed even for small surface viscosities. The torque coefficient is not very sensitive to k and e, especially for high values of those parameters [Fig. 16(b)]. The curve for $k = e = 100$ practically coincides with that which refers to a solid wall.

Figure 17 illustrates the surface viscosity effect and its connection with the distance between the particle

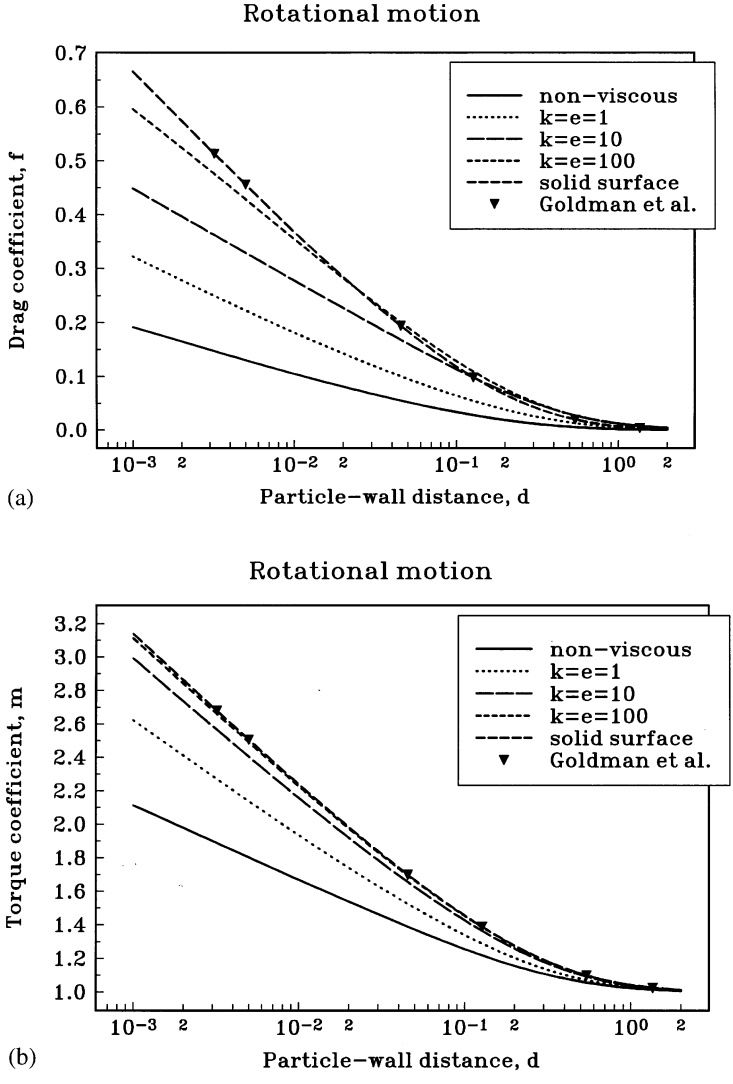

Fig. 16. (a) Deimensionless drag coefficient for rotation, as a function of the particle–wall distance; (b) dimensionless torque coefficient for rotation, as a function of the particle–wall distance.

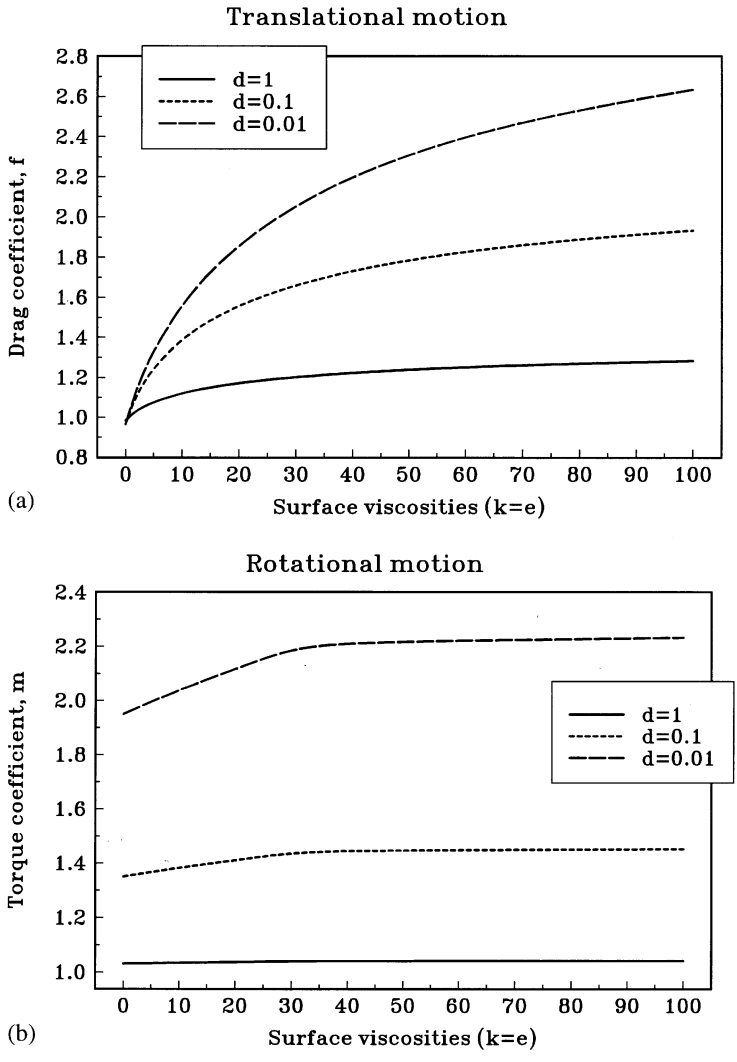

Fig. 17. (a) Dimensionless drag coefficient for translation, as a function of the surface viscosity, $k = e$, $\beta = \eta_2/\eta_1 = 0.907$; (b) dimensionless torque coefficient for rotation, as a function of the surface viscosity, $k = e$, $\beta = \eta_2/\eta_1 = 0.907$.

and the liquid interface. We see that for small d the influence of the surface viscosity is quite substantial for translation. In the case of rotation d is the predominant factor determining the torque [Fig. 17(b)]. It is not surprising that at $d = 1$ the surface viscosity is virtually immaterial and $m \approx 1$. Indeed, for rotation the fluid motion is confined in a narrow zone around the sphere and the velocity decays very fast (cf. Fig. 4). We study also the role of the *bulk* viscosity, varying β with $k = e = 0$, Fig. 18. The numerical values for f and m are comparable in magnitude to those obtained at different surface viscosities (cf Fig. 17). Again the particle–wall distance is found to be of major importance, when it is small β becomes a factor of increasing influence. If the phase Ω_2 is a gas ($\beta = 0$), then the drag associated with translation falls markedly below 1 [Fig. 18(a)].

The stationary velocities of the two elementary motions of the solid sphere when it is subjected to buoyancy force are plotted in Fig. 19. The translation is considerably retarded when the interface is viscous and d is small. On the other hand, with lower bulk viscosity in the region Ω_2 and with vanishing surface viscosity the particle can move faster compared to the case of unbounded liquid ($V_c > V_{\text{Stokes}}$). Generally, the rotation turns out to be quite slow—Fig. 19b. Its *direction* can change depending on the surface viscosity. One may easily foresee that near the viscous or solid wall the vector of the angular velocity will point to the negative x-axis. Both for translation and for rotation $k = e = 100$ leads to results close to those when the surface S_2 is rigid. Finally, one can discuss the role of the bulk viscosity (that is, β). Data are presented in Fig. 20 for $k = e = 0$. Again, the effects of

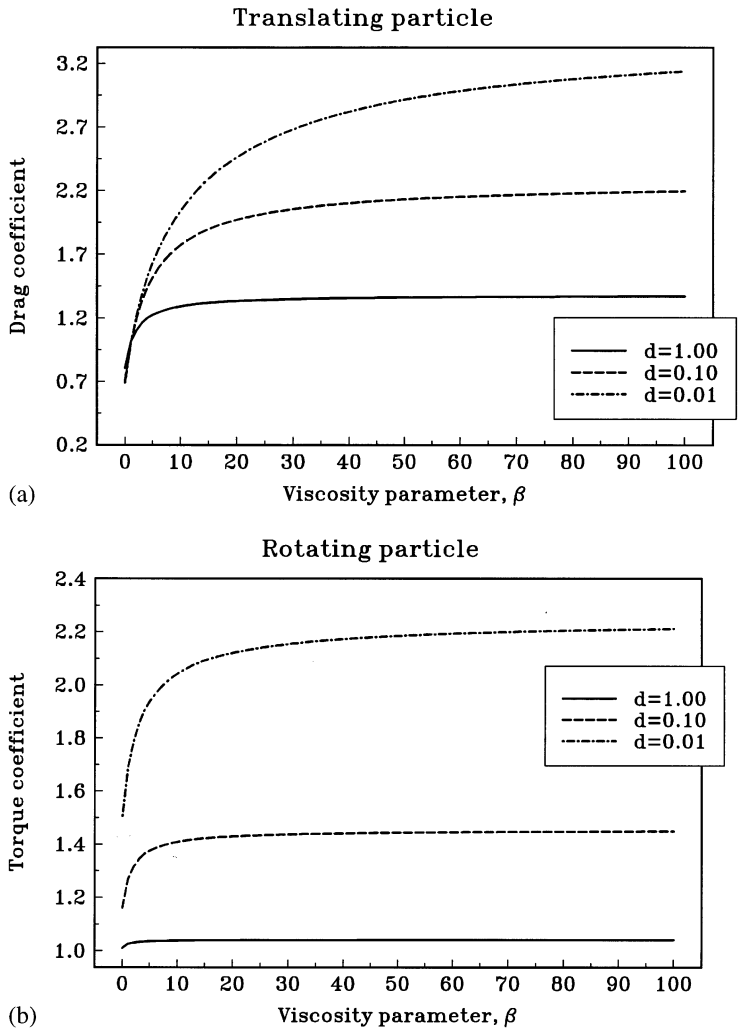

Fig. 18. (a) Dimensionless drag coefficient for translation, as a function of the bulk viscosity parameter, $\beta = \eta_2/\eta_1$, $k = e = 0$; (b) dimensionless torque coefficient for rotation, as a function of the bulk viscosity parameter, $\beta = \eta_2/\eta_1$, $k = e = 0$.

d and β are interrelated. The cases of highly viscous phase Ω_2 (large β), and gaseous phase ($\beta = 0$) are clearly distinguished. At small values of β one observes $V_c > V_{\text{Stokes}}$ and $\omega_c > 0$.

6. CONCLUDING REMARKS

This article is focused on the role of the intrinsic viscous properties of a liquid surface, which influences the flow in the two adjacent bulk phases. The creeping motion caused by a rigid sphere which translates or rotates parallel to the interface is considered. The liquid boundary is supposed to be Newtonian, it possesses dilatational and shear surface viscosities. The stress on it obeys the Boussinesq–Scriven constitutive relation. To solve the hydrodynamic problem we apply a method similar to that used previously by other authors for solid or non-viscous interfaces. The boundary condition for the tangential stress balance is augmented with account for the viscous friction within the surface. The velocity components and the pressure in the fluid, as well as the drag and the torque experienced by the particle, are determined numerically.

At small distances between the sphere and the wall, one observes a substantial influence of the surface viscosity: it leads to increase of the drag and torque, and retards the motion when a constant external force (for example, buoyancy) is applied to the particle. For steady rotation the flow around the solid sphere is restrained in a narrow region, whereas in the case of translation the velocity field extends to large distances. Consequently, the rotating particle should be closer in order to start 'feeling' the liquid interface.

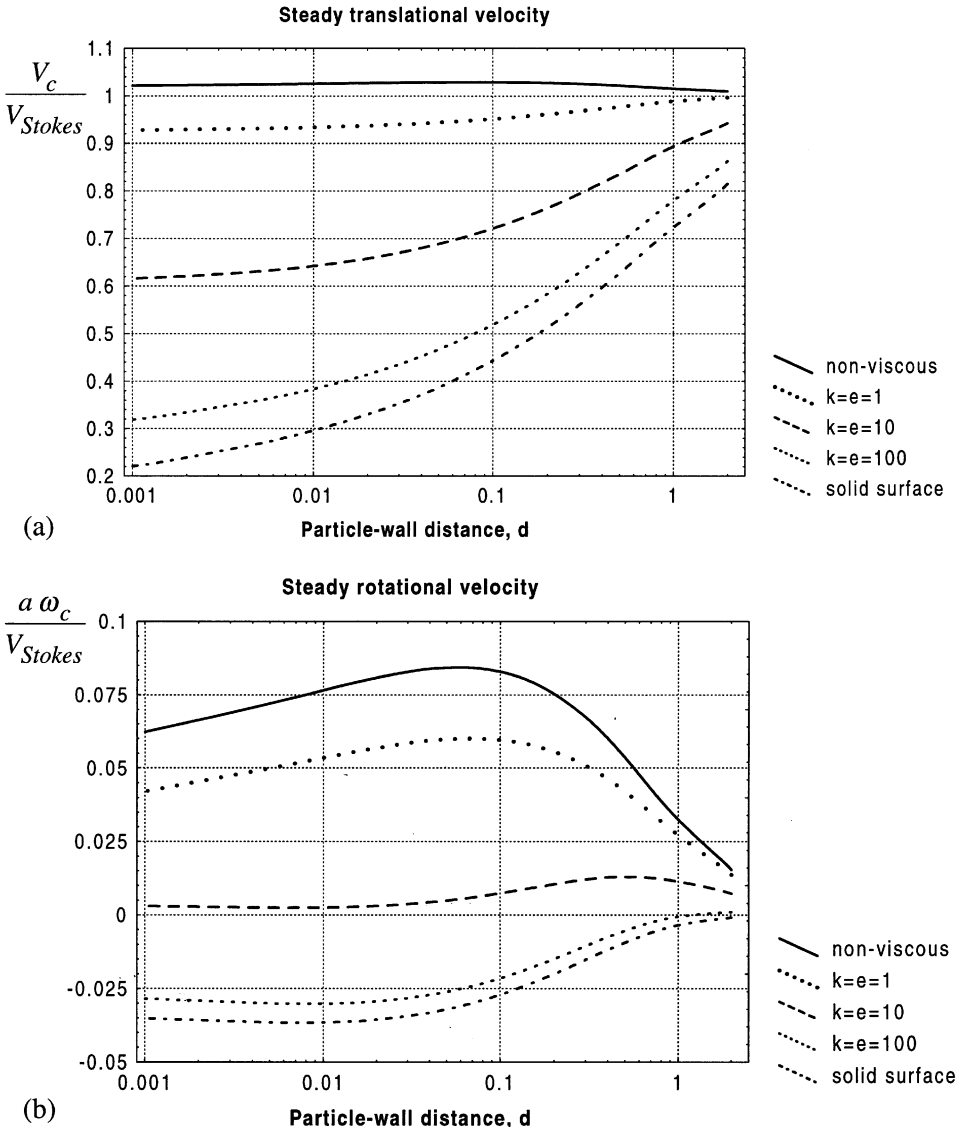

Fig. 19. (a) Velocity of stationary translation of the particle under the action of gravity, scaled by the Stokes velocity in an unbounded fluid, as a function of the particle–wall distance; (b) angular velocity of stationary rotation of the particle under the action of gravity force, times the radius, scaled by the Stokes velocity in an unbounded fluid, as a function of the particle–wall distance.

The bulk viscosity is found to play a role as well. If the phase beyond the wall is less viscous, and for small *surface* viscosity, the drag can be smaller than that corresponding to motion in an unbounded liquid. The torque can change its sign depending on the properties of the bulk and the interface.

Our results can be important for systems which contain surfactant-loaded liquid boundaries. Such a boundary can affect the motion of a micron-sized particle in much the same way as a solid wall—see the estimtes in Section 5 above. The influence can be substantial even with low molecular weight surfactants, it should be particularly high for adsorbed proteins, as the latter immobilise the liquid interface completely.

Many experimental methods for measuring the interfacial viscosities have been developed, some of them are reviewed by Edwards *et al.* (1991). We shall mention here a recent work which opens a new route to solving this problem, being to some extent connected with the results described in the present paper. Petkov *et al.* (1995) were able to obtain the drag coefficient by measuring the particle velocity and calculating the lateral capillary force which is operative when a solid sphere is attached to a liquid surface. (The particle is partially immersed in both phases and forms a contact angle.) Having found the drag coefficient, one may rely on theoretical computations to fit the value using certain interfacial viscosity numbers. This can represent a new method for determination of

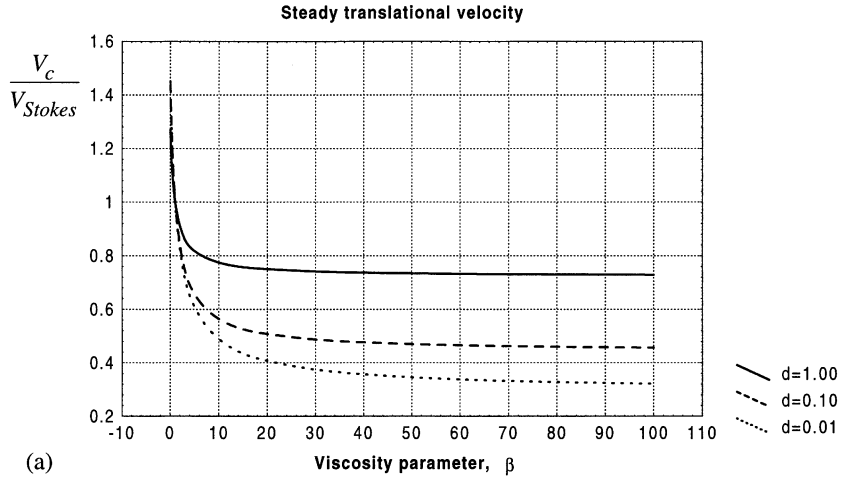

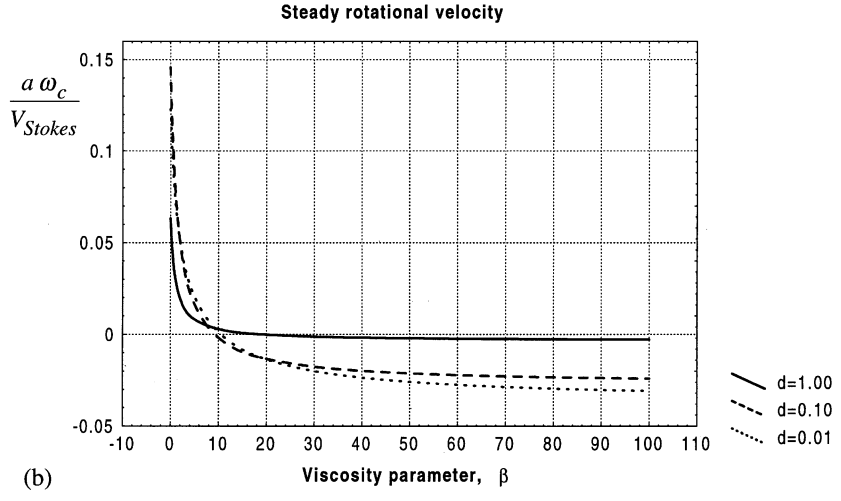

Fig. 20. (a) Velocity of stationary translation of the particle under the action of gravity, scaled by the Stokes velocity in an unbounded fluid, as a function of the bulk viscosity parameter, $\beta = \eta_2/\eta_1$, $k = e = 0$; (b) angular velocity of stationary rotation of the particle under the action of gravity force, times the radius, scaled by the Stokes velocity in an unbounded fluid, as a function of the bulk viscosity parameter, $\beta = \eta_2/\eta_1$, $k = e = 0$.

the surface viscosity. Similar ideas can be applied for the case of a particle attached below or above the liquid boundary without touching it (for example, under the action of gravity force). Then, the calculations included in this article will be of help in order to interpret the data for the drag coefficient.

Acknowledgements

The present work was financially supported by the 'Volkswagen-Stiftung'. The authors gratefully acknowledge this support of their collaborative research. TG wishes to express sincere appreciation for the hospitality of the LSTM-Erlangen during his stay there.

REFERENCES

Arfken, G. (1985) *Mathematical Methods for Physicists.* Academic Press, Boston.

Berdan, C. II and Leal, L. G. (1982) Motion of a sphere in the presence of a deformable interface. I. Perturbation of the interface from flat: the effects on drag and torque. *J. Colloid Interface Sci.* **87**, 62–80.

Boussinesq, M. J. (1913) Sur l'éxistance d'une viscosité superficielle, dans la mince couche de transition separant un liquide d'une autre fluide contigue. *Ann. Chim. Phys.* **29**, 349–357.

Cooley, M. D. A. and O'Neill, M. E. (1968) On the slow rotation of a sphere about a diameter parallel to a nearby plane wall. *J. Inst. Math. Appl.* **4**, 163–173.

Danov, K. D., Aust, R., Durst, F. and Lange, U. (1995) Influence of the surface viscosity on the drag and torque coefficients of a solid particle in a thin liquid layer. *Chem. Engng Sci.* **50**, 263–277.

Dean, W. R. and O'Neill, M. E. (1963) A slow motion of viscous liquid caused by a slowly rotating solid sphere. *Mathematika* **10**, 13–24.

Edwards, D. A., Brenner, H. and Wasan, D. T. (1991) *Interfacial Transport Processes and Rheology*. Butterworth–Heinemann, Boston.

Faxén, H. (1921) Dissertation. Uppsala University.

Goldman, A. J., Cox, R. G. and Brenner, H. (1967) Slow viscous motion of a sphere parallel to a plane wall. *Chem. Engng Sci.* **22**, 637–651.

Graham, D. E. and Phillips, M. C. (1980a) Proteins at liquid interfaces. IV. Dilatational properties. *J. Colloid Interface Sci.* **76**, 227–239.

Graham, D. E. and Phillips, M. C. (1980b) Proteins at liquid interfaces. V. Shear properties *J. Colloid Interface Sci.* **76**, 240–250.

Happel, J. and Brenner, H. (1965) *Low Reynolds Number Hydrodynamics with Special Applications to Particulate Media*. Prentice-Hall, Englewood Cliffs, NJ.

Hunter, R. J. (1987) *Foundations of Colloid Science*, Vol. 1, pp. 608–611. Clarendon Press, Oxford.

Jahnke, E., Emde, F. and Lösch, F. (1960) *Tafeln Höherer Funktionen*. B. G. Teubner Verlagsgesellschaft, Stuttgart.

Kim, S. and Karrila, S. J. (1991) *Microhydrodynamics: Principles and Selected Applications*. Butterworth-Heinemann, Boston.

Lamb, H. (1945) *Hydrodynamics*. Dover, New York.

Lee, S. H. and Leal, L. G. (1980) Motion of a sphere in the presence of a plane interface. Part 2. An exact solution in bipolar co-ordinates. *J. Fluid Mech.* **98**, 193–224.

O'Neill, M. E. (1964) A slow motion of viscous liquid caused by a slowly moving solid sphere. *Mathematika* **11**, 67–74.

O'Neill, M. E. and Ranger, K. B. (1979) Rotation of a sphere in two phase flow. *Int. J. Multiphase Flow* **5**, 143–148.

O'Neill, M. E. and Stewartson, K. (1967) On the slow motion of a sphere parallel to a nearby plane wall. *J. Fluid Mech.* **27**, 705–724.

Petkov, J. T., Denkov, N. D., Danov, K. D., Velev, O. D., Aust, R. and Durst, F. (1995) Measurement of the drag coefficient of spherical particles attached to fluid interfaces. *J. Colloid Interface Sci.* **172**, 147–154.

Scriven, L. E. (1960) Dynamics of a Fluid Interface. *Chem. Engng Sci.* **12**, 98–108.

Shapira, M. and Haber, S. (1988) Low Reynolds number motion of a droplet between two parallel flat plates. *Int. J. Multiphase Flow* **14**, 483–506.

Shapira, M. and Haber, S. (1990) Low Reynolds number motion of a droplet in shear flow including wall effects. *Int. J. Multiphase Flow* **16**, 305–321.

Slattery, J. C. (1990) *Interfacial Transport Phenomena*. Springer, New York.

Smoluchowski, M. (1911) On the mutual action of spheres which move in a viscous liquid. *Bull. Acad. Sci. Cracovie A* **1**, 28–39.

Stokes, G. G. (1851) On the effect of the internal friction of fluids on the motion of a pendulum. *Trans. Cambridge Phil. Soc.* **1**, 104–106.

Wakiya, S. (1956) *Res. Rep. Fac. Engng Niigata University, Japan* **5**, 1.